SIAM J. APPL. MATH.
Vol. 63, No. 1, pp. 62–97

MULTIPLE BUMPS IN A NEURONAL MODEL OF WORKING MEMORY*

CARLO R. LAING†, WILLIAM C. TROY‡, BORIS GUTKIN§, AND G. BARD ERMENTROUT‡

Abstract. We study a partial integro-differential equation defined on a spatially extended domain that arises from the modeling of "working" or short-term memory in a neuronal network. The equation is capable of supporting spatially localized regions of high activity which can be switched "on" and "off" by transient external stimuli. We analyze the effects of coupling between units in the network, showing that if the connection strengths decay monotonically with distance, then no more than one region of high activity can persist, whereas if they decay in an oscillatory fashion, then multiple regions can persist.

Key words. short-term memory, integro-differential equation, coupling, homoclinic orbits

AMS subject classifications. 34B15, 34C23, 93C15, 34C11

PII. S0036139901389495

1. Introduction.

Working memory, which involves the holding and processing of information on the time scale of seconds, is a much studied area of neuroscience [3, 9, 24, 35, 37]. Experiments in primates [8, 15, 29] have shown that there exist neurons in the prefrontal cortex that have elevated firing rates during the period in which an animal is "remembering" the spatial location of an event before acting on the information being remembered. Realistic models for this type of activity have involved spatially extended systems of coupled neural elements and the study of spatially localized areas of high activity in these systems. Previous studies have involved "rate" models [1, 19, 22, 37] in which a neural element is described by a single scalar variable, e.g., a firing rate and more complicated "spiking" models [9, 24, 35], which take into account the intrinsic dynamics of single neurons.

In this paper we extend the 1977 work of Amari [1] who found *single* spatially localized regions of high activity ("bumps") in rate models of the form

$$\frac{\partial u(x,t)}{\partial t} = -u(x,t) + \int_{-\infty}^{\infty} w(x-y) f(u(y,t))\, dy + s(x,t) + h. \tag{1.1}$$

Equation (1.1) models a single layer of neurons. The function $u(x,t)$ denotes the "synaptic drive" or "synaptic input" to a neural element at position $x \in (-\infty, \infty)$ and time $t \geq 0$. The connection function $w(x)$ determines the coupling between elements, and the nonnegative function $f(u)$ gives the firing rate, or activity, of a neuron with input u. Neurons at a point x are said to be active if $f(u(x,t)) > 0$. The function $s(x,t)$ represents a variable external stimulus. Finally, the parameter h denotes a *constant* external stimulus applied uniformly to the entire neural field. Although

*Received by the editors May 16, 2001; accepted for publication (in revised form) February 15, 2002; published electronically August 5, 2002.
http://www.siam.org/journals/siap/63-1/38949.html
†Department of Physics, University of Ottawa, Ottawa ON, Canada K1N 6N5 (claing@science.uottawa.ca).
‡Department of Mathematics, University of Pittsburgh, Pittsburgh, PA 15260 (troy@vms.cis.pitt.edu, bard@pitt.edu).
§Unité de Neurosciences Intergratives et Computationelles, CNRS, Gif-sur-Yvete 91198, France (gutkin@cnbc.cmu.edu).

the model we study has been used to model working memory, similar equations arise in neural theory as applied to vision and robotic navigation [17], head direction systems [39], and cognitive development in infants [32]. We also mention recent analyses of wave propagation when inhomogeneities are present in the underlying neural substrate [4] and also in neural networks with axo-dendritic synaptic interactions [10].

Our goal is to extend Amari's results in two ways. First, in the next section we will extend the analysis of the original model in which $w(x)$ is assumed to have exactly one zero in $(0,\infty)$, and $f(u)$ is a step function. We will determine a simple set of assumptions on w and f for which (1.1) has stationary "single-bump" solutions. Our assumptions will allow us to obtain a more precise description of the shape of solutions. We will also investigate the existence of "double-bump" solutions.

In section 3 we relax the restrictions on w and f to include both oscillatory connection functions which change sign infinitely often and *continuous* firing rate functions. Our goal here is to show that "multi-bump" solutions of (1.1) exist over an appropriate range of parameters. The extension of $f(u)$ to a continuous function will allow us to derive an ordinary differential equation, specific solutions of which are steady-states of (1.1). This differential equation, which is derived in section 5, will be invaluable in proving the existence or otherwise of such "multi-bump" solutions. Sections 6 and 7 are devoted to studies of its N-bump solutions. In section 8 we extend the model to two space dimensions and present numerical evidence for multi–bumps solutions. Sections 9 and 10 contain proofs of two theorems stated in the text, and a summary of our results is given in section 11.

2. "Mexican hat" coupling. We begin with a description of the assumptions and conclusions obtained by Amari [1] where the coupling function $w(x)$ satisfies the following:

(H_1) $w(x)$ is symmetric, i.e., $w(-x) = w(x)$ for all $x \in \mathbf{R}$;
(H_2) $w(x) > 0$ on an interval $(-\bar{x}, \bar{x})$, and $w(-\bar{x}) = w(\bar{x}) = 0$;
(H_3) $w(x)$ is decreasing on $(0, \bar{x}]$;
(H_4) $w < 0$ on $(-\infty, -\bar{x}) \cup (\bar{x}, \infty)$.

An additional condition which Amari uses but does not explicitly state is

(H_5) w is continuous on $\mathbf{R}$, and $\int_{-\infty}^{\infty} w(y)\,dy$ is finite.

A coupling satisfying (H_2) and (H_4) produces "lateral inhibition" [14]. That is, condition (H_2) means that nearby neural elements excite one another, but (H_4) results in an "inhibitory effect" if the distance between neural elements is greater than a certain value, $\bar{x}$. Conditions (H_1), (H_3) and (H_5) are general requirements which allow for a tractable mathematical analysis of (1.1). In order to rigorously determine the shape of steady-state solutions of (1.1), we make one final assumption on the coupling function $w(x)$:

(H_6) $w(x)$ has a unique minimum on $\mathbf{R}^+$ at a point $x_0 > \bar{x}$, and $w(x)$ is strictly increasing on (x_0, ∞).

A connection function which satisfies conditions (H_1)–(H_6) is

$$w(x) = Ke^{-k|x|} - Me^{-m|x|}, \tag{2.1}$$

where $0 < M < K$ and $0 < m < k$. An example of this "Mexican hat" type function is given in Figure 1 for $K = 3.5$, $M = 3$, $k = 1.8$, and $m = 1.52$. For simplicity, Amari assumes (see Figure 1) that the firing rate $f(u)$ is the Heaviside step function

$$f(u) = \begin{cases} 0, & u \le 0, \\ 1, & u > 0. \end{cases} \tag{2.2}$$

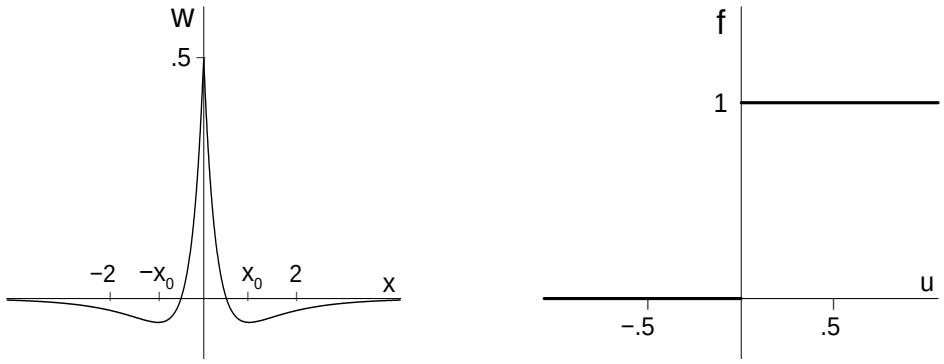

FIG. 1. *Mexican hat function* (2.1) *for parameters given in the text, and the Heaviside firing rate function* (2.2).

The effect of (2.2) is that a neuron fires at its maximum rate when the input exceeds the threshold value $u = 0$ and does not fire otherwise. Thus, (2.2) can be viewed as modeling neural elements whose firing rates "saturate" immediately, since increasing the input further does not cause the firing rate to increase, provided the input is above the threshold value.

Under assumptions (H_1)–(H_5), Amari analyzes the existence and stability of equilibrium solutions of (1.1) under the assumption that there is no "inhomogeneous" external stimulus $s(x,t)$. That is, he sets $\partial u(x,t)/\partial t = 0$ and $s(x,t) = 0$. This reduces (1.1) to the time independent equation

$$u(x) = \int_{-\infty}^{\infty} w(x-y) f(u(y))\, dy + h. \tag{2.3}$$

Solutions of (2.3) are called equilibrium or *stationary* solutions. An important observation is that the neural system is still subject to the constant external stimulus h applied uniformly to the entire neural field. Note that if $h \leq 0$, then the constant function $u = h$ is a solution of (2.3).

Single-bump solutions: For a given distribution $u(x)$, Amari defines its region of excitation to be the set

$$R(u) = \{x | u(x) > 0\}.$$

He then defines a *localized excitation* to be a pattern $u(x)$ whose region of excitation is a *finite* interval, i.e., $R(u) = (a_1, a_2)$. If $R(u)$ is connected, we refer to the pattern as a "single-bump", or "1-bump" solution. Furthermore, because (2.3) is homogeneous, it is easily verified that $u(x-a)$ is a solution whenever $u(x)$ is a solution. Thus, without loss of generality, we assume that the region of excitation for a single-bump solution has the form

$$R(u) = (0, a).$$

Remark. If (2.3) has a solution whose region of excitation consists of $N > 1$ disjoint, finite connected intervals, the solution is called an *N-bump* solution. A major goal of this paper is to show that multi-bump solutions exist for (2.3) when the restrictions on $w(x)$ and $f(u)$ are relaxed.

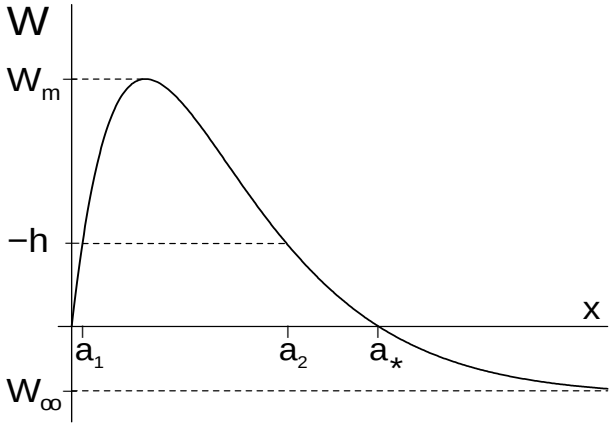

FIG. 2. $W(x)$, (2.4), *for parameters given in the text. We have chosen* h *to be negative, so that* $W_\infty < 0 < -h < W_m$.

In his analysis of single-bump solutions, Amari makes use of the function

$$W(x) = \int_0^x w(y)\,dy \tag{2.4}$$

and the related quantities

$$W_m = \max_{x>0} W(x) \quad \text{and} \quad W_\infty = \lim_{x\to\infty} W(x). \tag{2.5}$$

Conditions (H_1) and (H_5) imply that $W(x)$ is odd, and that W_∞ is finite, respectively. Amari observes that if (2.3) has a single-bump solution $u(x)$ whose region of excitation is given by $R(u) = (0, a)$, then $u(x)$ satisfies

$$u(x) = \int_0^a w(x-y)\,dy + h = W(x) - W(x-a) + h. \tag{2.6}$$

At the value $x = a$, (2.6) reduces to

$$W(a) = -h \tag{2.7}$$

since $W(x)$ is odd and $u(0) = u(a) = 0$. In turn, Amari claims that if $a > 0$ and $h < 0$ satisfy (2.7), then

$$u(x) = W(x) - W(x-a) + h \tag{2.8}$$

is a single-bump solution of (2.3) for which $R(u) = (0, a)$.

For a given $h \le 0$, (2.7) may have zero, one or two positive solutions. The exact number is determined by the relative values of W_∞, W_m, and h. In Figure 2 we construct the $W(x)$ corresponding to the Mexican hat function illustrated in Figure 1. That is, we use the formula for $w(x)$ given in (2.1) for the specific values $K = 3.5$, $k = 1.8$, $M = 3$, and $m = 1.52$. In Figure 2 we see that if $W_\infty < 0 < -h < W_m$, then there are two values, a_1 and a_2, which satisfy (2.7). Setting $a = a_1$ and $a = a_2$ in (2.8)

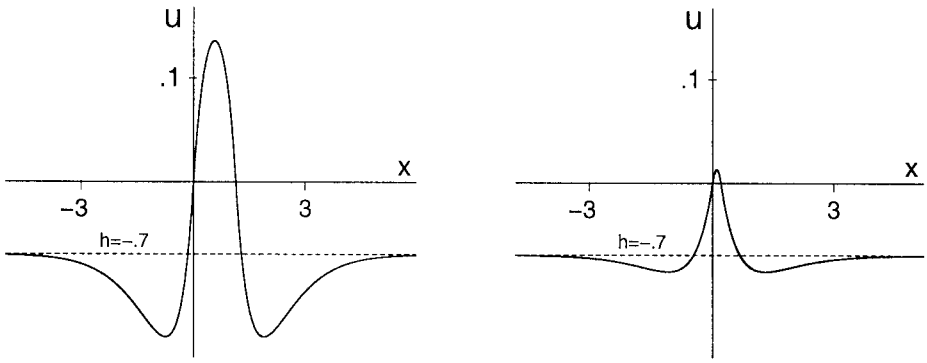

FIG. 3. *Stable (left) and unstable (right) single-bump solutions of* (2.3) *for the functions* w *and* f *shown in Figure* 1 *and* $h = -0.7$.

gives the corresponding single-bump solutions of (2.3). In Figure 3 we illustrate these two solutions for the value $h = -0.7$. Amari gives arguments that indicate that the large amplitude solution corresponding to $a = a_2$ (i.e., the first solution in Figure 3) is stable, while the second, smaller amplitude solution in Figure 3 corresponding to $a = a_1$ is unstable. Furthermore, as Figure 2 indicates, if $h = 0$, then (2.7) holds only at the positive value $a = a_2 = a_*$. Setting $a = a_*$ and $h = 0$ in (2.8), one can easily show that the resulting function is still a single-bump solution of (2.3).

We note that if (2.7) has a solution for some $a > 0$ and $h > 0$, then (2.8) implies that $u(x) > 0$ for all large x, contradicting the supposition that $R(u) = (0, a)$ is finite. Thus, single-bump solutions do not exist if $h > 0$.

Finally, we make a few observations concerning the *shape* of nonconstant single-bump solutions (see Figure 3). First, we conclude from hypotheses (H_1)–(H_4) and (2.8) that $u(x)$ is symmetric with respect to $x = a/2$ and that $u(x)$ is increasing on $(0, a/2)$ and decreasing on $(a/2, a)$. When we consider the additional hypotheses (H_5) and (H_6), it follows from standard analysis that the solution $u(x)$ has a unique minimum on $(0, \infty)$, and that $u(x) \to h$ from below as $x \to \infty$.

Double-bump solutions: We now consider the possible existence of double-bump solutions. A solution $u(x)$ of (2.3) is called a double-bump, or 2-bump, solution if there are values $0 < a < b < c$ such that

$$\begin{cases} u > 0 \quad \text{on} \quad (0, a) \cup (b, c), \\ u(0) = u(a) = u(b) = u(c) = 0, \\ u < 0 \quad \text{otherwise.} \end{cases} \tag{2.9}$$

Thus, a 2-bump solution is one whose region of excitation consists of two disjoint, connected intervals. The quantity $b - a$ is the distance between bumps. Our goal is to prove the existence or nonexistence of double-bump solutions of (2.3) which satisfy property (2.9). In general, a rigorous resolution of this problem is very difficult. Before stating our first result, we recall that x_0 denotes the unique positive value at which the coupling function $w(x)$ attains its global minimum and that $w(x)$ is strictly increasing on (x_0, ∞) (see Figure 1). In the following result we eliminate a class of 2-bump solutions.

THEOREM 2.1. *Under hypotheses* (H_1)–(H_6) *there is no value* $h \in \mathbf{R}$ *for which the problem* (2.2)–(2.3) *has a* 2*-bump solution such that the distance between bumps satisfies* $b - a \geq x_0$.

Remark. Theorem 2.1 does not completely eliminate the existence of all double-bump solutions. For example, our proof does not address the existence of general 2-bump solutions such that the distance $b - a$ satisfies $b - a < x_0$. However, it can be shown that under the assumptions $c - b = a$, i.e., equal width bumps, and $W_\infty < 0$, (2.2)–(2.3) can support (possibly unstable) 2-bump solutions [33] (and see [18]). We also have no results concerning existence or nonexistence of N-bump solutions where $N \geq 3$. The resolution of these problems remains open.

Because the proof of Theorem 2.1 is somewhat technical, we postpone the details until section 9. We proceed in the next section to describe the main focus of our investigation.

3. Statement of main results. The main goal of our investigation is to extend the analysis in section 2 and determine conditions on the connection and firing functions so that the integral equation (1.1) has stable *N-bump* solutions. For this we choose a specific $w(x)$ which changes sign infinitely often, and we let $f(u)$ be a continuous extension of the Heaviside function. For simplicity it is assumed that both $s(x,t) = 0$ and $h = 0$. Setting $h = 0$ will be compensated for by including a threshold in f. Thus, we study the problem

$$\frac{\partial u(x,t)}{\partial t} = -u(x,t) + \int_{-\infty}^{\infty} w(x-y) f(u(y,t))\, dy, \tag{3.1}$$

where

$$w(x) = e^{-b|x|}(b \sin|x| + \cos x) \tag{3.2}$$

and

$$f(u) = 2e^{-r/(u-th)^2} H(u - th). \tag{3.3}$$

Here $th > 0$, $b > 0$, and $r > 0$ are constants. The parameter b controls the rate at which the oscillations in w decay with distance. As shown in Figure 4, they decay more rapidly as b is increased. It is hoped that this oscillatory form of coupling better represents the connectivity known to exist in the prefrontal cortex, where labeling studies have shown that coupled groups of neurons form spatially approximately periodic stripes [16, 26, 27]. Interestingly, it has been proposed that disruption of this "lattice" of connectivity may be responsible for some of the symptoms of schizophrenia [27]. Note that we are not addressing the processes involved in the *formation* of these stripes, but are interested in the possible patterns of neural activity that can exist in the system once these patterns are in place. Also, although $w(x)$ does not have finite support we know that in the brain, connections cannot exist over arbitrarily large distances, so this is obviously an approximation to reality. It would be an interesting problem to analyze (3.1) with a function $w(x)$ that had more than one zero crossing for $x > 0$ yet had finite support. Finally, it is interesting to observe that the coupling given in (3.2) is differentiable at $x = 0$, and that $w'(0) = 0$. This is proved in [23] and easily follows from the formal definition of derivative. In contrast, the lateral inhibition coupling given in (2.1) is not differentiable at $x = 0$. However, we believe that the only significant feature for analysis of the models is continuity of w at $x = 0$.

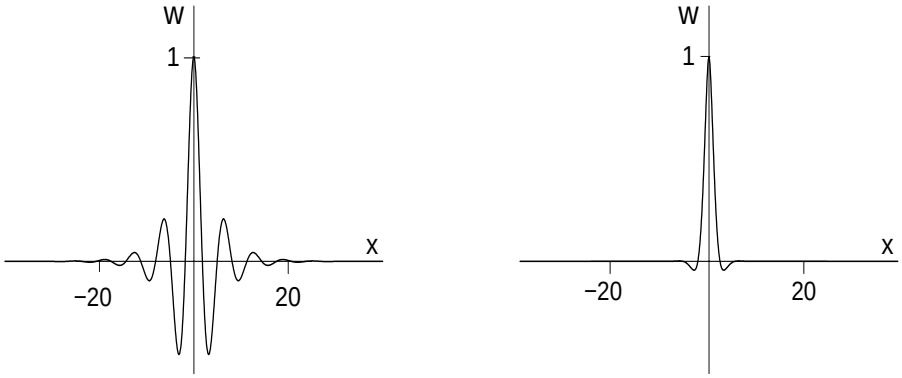

FIG. 4. $w(x)$, (3.2), *for* $b = 0.25$ *(left) and* $b = 1.0$ *(right).*

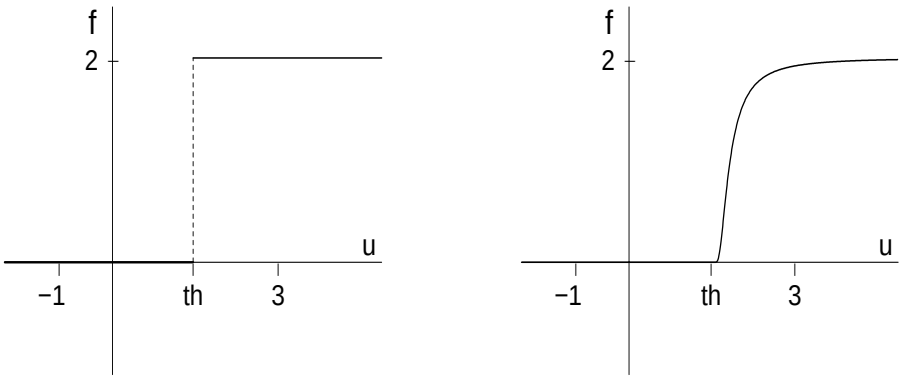

FIG. 5. $f(u)$, (3.3), *for* $r = 0$ *(left) and* $r = 0.1$ *(right), with* $th = 1.5$.

The parameter th denotes the *threshold* that is now included in $f(u)$. The coefficient of 2 in (3.3) was chosen merely for convenience. We note that $f(u) = 0$ if and only if $u \leq th$. Furthermore, $f(u)$ is a C^∞ function when $r > 0$, and r controls the rate of increase of $f(u)$ for u just past threshold. The differentiability of f will be useful when we derive a differential equation, specific solutions of which are equivalent to steady-state solutions of (3.1). In Figure 5 we set $th = 1.5$ and graph $f(u)$ for $r = 0$ (left) and $r = 0.1$ (right). When $r = 0$, $f(u)$ is just twice the Heaviside function. For $r > 0$, $f(u)$ is a *continuous* function which rapidly approaches 2 from below as u increases past th.

The choice of the functions (3.2) and (3.3) had some arbitrariness to it. The important features of (3.3) are that $f(u) = 0$ for $u \leq th$ and that $f(u)$ is sufficiently differentiable. The choice of (3.2) was made not only because it has the appropriate shape (decaying oscillations, with approximately the same distance between successive maxima), but also because the form of its Fourier transform makes the ordinary differential equation derived in section 5 particularly simple. Our hope is that the

qualitative details of the following results do not depend on the exact form of (3.2) and (3.3).

As before, we define a "stationary solution" to be a time independent solution of (3.1)–(3.3). Thus, a stationary solution satisfies the equation

$$u(x) = \int_{-\infty}^{\infty} w(x-y) f(u(y)) dy. \tag{3.4}$$

Before proceeding with our study of N-bump stationary solutions, we need to make precise the definition of the "region of excitation." For a solution of (3.4), we define its region of excitation to be the set

$$R(u) = \{x | u(x) > th\}. \tag{3.5}$$

A solution of (3.4) is an N-bump solution if its region of excitation consists of exactly N disjoint, finite connected intervals.

In the next section we begin our investigation of N-bump stationary solutions by considering the limiting value $r = 0$. As $r \to 0^+$ we note that the firing function tends to the discontinuous step function depicted in Figure 5 (left). In sections 5–7 we extend our studies to the case $r > 0$, for which the firing function $f(u)$ is *continuous.* As mentioned above, when $r > 0$ we find that there is an equivalent differential equation, some of whose solutions are solutions of (3.4). In section 5 we derive this fourth order equation and state our second theorem which determines a range of parameter values over which N-bump solutions can possibly exist. The differential equation will be especially useful to us in sections 6 and 7 where we give an extensive numerical investigation of the global behavior of entire families of N-bump solutions as parameters vary. Section 6 consists of a study of families of N-bump solutions for odd values of N, while section 7 covers even values of N.

4. The limiting problem: $r = 0$. It is natural to begin our investigation by considering the case $r = 0$ where $f(u)$ reduces to a multiple of the Heaviside function. In order to understand this case, we investigate the existence of N-bump solutions for a specific choice of the parameters b and th. For convenience we set $th = 1.5$ and $b = 0.25$ (see Figures 4 and 5 in the previous section). At these values our computations suggest that the problem (3.1)–(3.3) has at least four *stable* N-bump solutions. These are shown on the *left* in Figures 6–9, where the initial profile $u(x, 0)$ is represented by the dashed curve, and the solid curve represents $u(x, t)$ at $t = 60$. The formula for $u(x, 0)$ is given by

$$u(x,0) = \cos\left(\frac{Lx}{12.5\pi}\right) \exp\left(-\left(\frac{Lx}{12.5\pi}\right)^2\right), \quad -12.5\pi < x < 12.5\pi. \tag{4.1}$$

The parameter $L > 0$ allows us to vary the initial profile $u(x, 0)$. Equation (3.1) was numerically solved by spatially discretizing it on a uniform grid and then moving forward in time with an Euler step until convergence. The integral was approximated by a Reimann sum; note that the convolution can be performed more efficiently with a fast Fourier transform.

In the left panel in Figures 6 and 7 we set $L = 6$ and $L = 2.5$, and find that $u(x, t)$ approaches stable 1-bump and 2-bump solutions, respectively, as $t \to \infty$. Our computations imply that these also are solutions of

$$u(x) = \int_{-\infty}^{\infty} w(x-y) f(u(y)) dy. \tag{4.2}$$

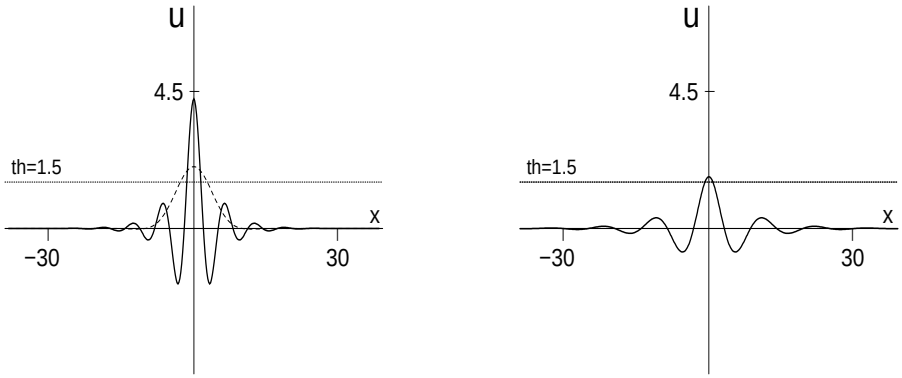

FIG. 6. *Stable (left) and unstable (right)* 1*-bump solutions:* $r = 0,\ th = 1.5,\ b = 0.25$.

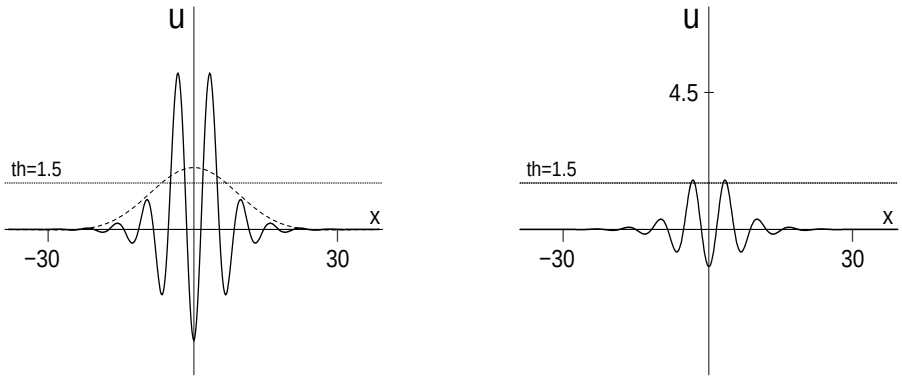

FIG. 7. *Stable (left) and unstable (right)* 2*-bump solutions:* $r = 0,\ th = 1.5,\ b = 0.25$.

Our computations also indicate that there exist *unstable* 1-bump and 2-bump stationary solutions. These are shown in the right panel in Figures 6 and 7. It is interesting to compare these unstable solutions with the unstable single-bump solution of the original Amari model described in section 2 (see Figure 3). Some of the stable solutions in Figures 6–9, Figures 14–17, Figure 19, Figure 23, Figures 25–28, and Figure 30 were found by numerically integrating (3.1) to a steady state, and the continuation program Auto97 [12, 13] was used to find the unstable solutions and reconfirm some of the stable solutions already found. We provide more detail in section 6.

Even though the system (3.1)–(3.3) is defined on an infinite domain, when numerically integrating (3.1) it must be finite. We have chosen a domain size of 25π, centered at $x = 0$. While it is unlikely that the boundaries have a significant effect on the spatially localized solutions shown in Figures 6 and 7, they will have a greater effect on broader solutions such as those in Figures 8 and 9. When comparing homoclinic orbits for the differential equation derived in section 5 (which represent solutions on an infinite domain) with solutions obtained from the numerical integration of (3.1),

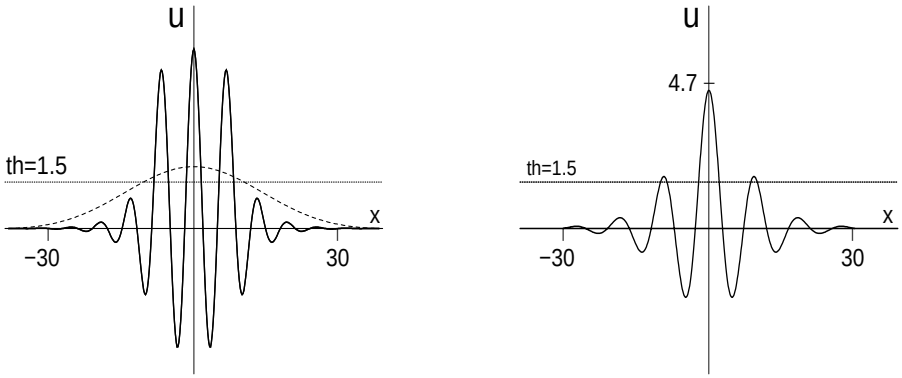

FIG. 8. *Stable (left) and unstable (right)* 3*-bump solutions:* $r = 0,\ th = 1.5,\ b = 0.25$.

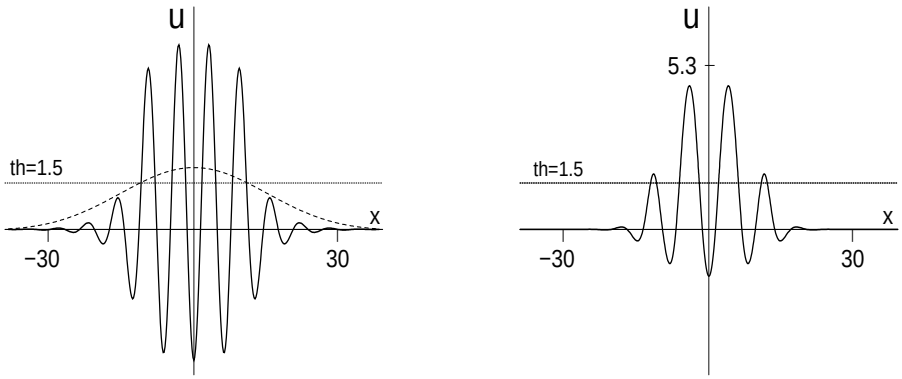

FIG. 9. *Stable (left) and unstable (right)* 4*-bump solutions:* $r = 0,\ th = 1.5,\ b = 0.25$.

the difference in domains should be kept in mind.

In the left panel of Figures 8 and 9 we let $L = 1.6$ and $L = 1.5$, respectively, and found that $u(x,t)$ tended to stable 3-bump and 4-bump stationary solutions as $t \to \infty$. Again, our computations indicate that there exist corresponding *unstable* 3-bump and 4-bump stationary solutions. These are shown in the right panels of Figures 8 and 9. Although we do not show the results, our computations indicate that if $L = 1$, then $u(x,t)$ tends to a stable 5-bump stationary solution as $t \to \infty$. For the values $r = 0$, $b = 0.25$, and $th = 1.5$, and a sufficiently large domain, we conjecture that both stable and unstable N-bump stationary solutions exist for each $N \geq 1$. We leave the resolution of this conjecture as an open problem.

We now develop a necessary mathematical criterion for the existence of 1-bump solutions of (4.2) when $r = 0$. In this case the firing function $f(u)$ defined in (3.3) reduces to twice the Heaviside function, as shown in the left panel of Figure 5. The solutions computed in Figures 6–9 are symmetric with respect to $x = 0$. Thus, we first look for single-bump *symmetric* solutions. We assume that there is a value $a > 0$

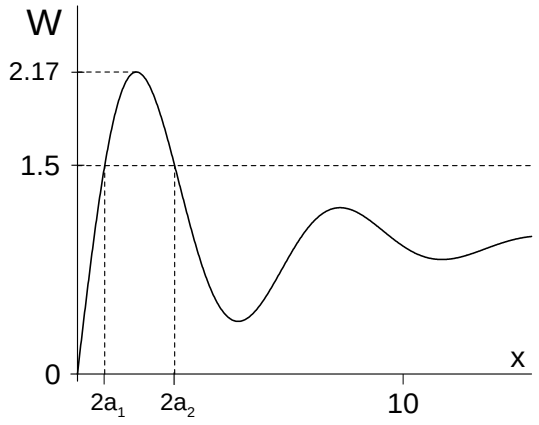

FIG. 10. $W(x)$, (4.4): $th = 1.5,\ b = 0.25$.

such that $u(x) > th$ on $(-a, a)$ and $u(x) < th$ if $|x| > a$. Under these assumptions, (4.2) reduces to

$$u(x) = \int_{-a}^{a} 2w(x-y)\,dy. \tag{4.3}$$

In analogy with section 2, we define

$$W(x) \equiv \int_{0}^{x} 2w(y)\,dy, \tag{4.4}$$

and note that $W(0) = 0$. From (4.3) and (4.4) it follows that

$$u(x) = W(x+a) - W(x-a). \tag{4.5}$$

Thus, we conclude that the condition $u(a) = th$ can be written as

$$W(2a) = th. \tag{4.6}$$

Figure 10 shows that, when $b = 0.25$ and $th = 1.5$, there are exactly two positive values, a_1 and a_2, for which (4.6) is satisfied. In Figure 11 we keep $th = 1.5$ and decrease b from $b = 0.25$. The left panel shows that there is a critical $b \approx 0.057$ at which a third value $a = a_3$ appears which satisfies $W(2a_3) = th$. For $0 < b < 0.057$ there are *at least* four solutions of (4.6). For example, we set $b = 0.03$ and illustrate this property in the right panel of Figure 11. As b decreases further, the number $\nu = \nu(b)$ of solutions of (4.6) (i.e., the number of symmetric 1-bump solutions of (4.2)) continues to increase, with $\nu(b) \to +\infty$ as $b \to 0^+$. In Figure 12 we see that the number $\nu(b)$ of solutions of (4.6) also increases if we keep b fixed at $b = 0.25$ and then lower the value of th from $th = 1.5$. Here we find that there is a critical value $th^* \equiv W(\infty) = 4b/(b^2+1)$ such that $\nu(b) \to +\infty$ as $th \to th^*$. We conjecture that each solution of (4.6) corresponds to a single-bump solution of the integral equation

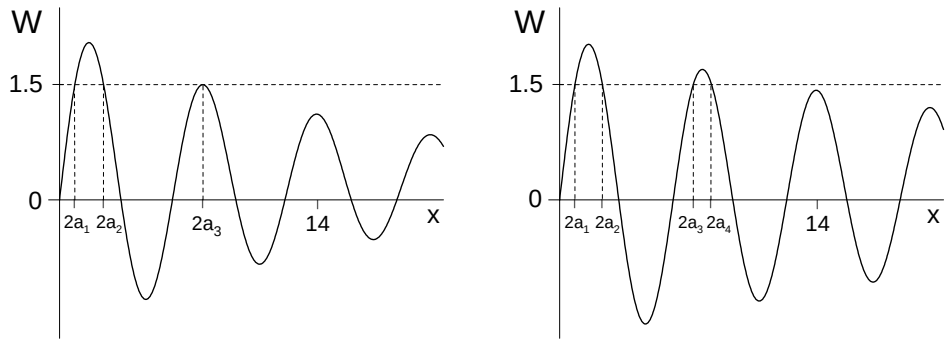

FIG. 11. $W(x)$, (4.4): $th = 1.5$; $b = 0.057$ *(left) and* $b = 0.03$ *(right).*

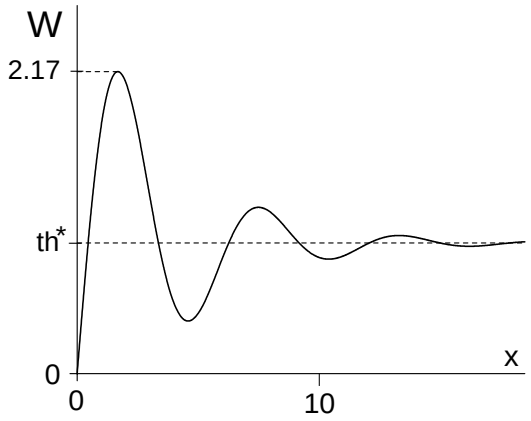

FIG. 12. $W(x)$, (4.4): $b = 0.25$, $th^* = 0.94$.

(4.2). In order to prove this conjecture, one would need to check that for all values of a satisfying (4.6), the function defined in (4.5) satisfied

$$u(x) > th \text{ for } -a < x < a \text{ and } u(x) < th \text{ for } x < -a \text{ or } a < x, \tag{4.7}$$

i.e., that the form of $u(x)$ given in (4.5) is actually a 1-bump solution. It would also be interesting to develop a criterion for the existence of N-bump solutions when $N > 1$. We leave these questions as open problems for future research.

5. The continuous case: $r > 0$. We now turn to the case $r > 0$, for which $f(u)$ is a *continuous* function. Thus, we study the existence of N-bump solutions of the equation

$$u(x) = \int_{-\infty}^{\infty} w(x-y) f(u(y))\, dy, \tag{5.1}$$

where $w(x)$ is given in (3.2) and $f(u)$ is given by (3.3), with $r > 0$. When $r > 0$, both the mathematical and computational analysis of (5.1) become more tractable. This is due to the fact that N-bump solutions of an associated differential equation problem also are solutions of (5.1). To derive the differential equation we make use of the Fourier transform, defined by

$$\mathrm{F}(g) = \int_{-\infty}^{\infty} e^{-i\alpha\eta} g(\eta)\, d\eta, \tag{5.2}$$

where $g \in L^1(\mathbf{R})$ and $\alpha \in \mathbf{R}$. Note that $\mathrm{F}(g)$ is a function of α.

We assume that u is a solution of (5.1), that u, u', u'', u''', and u'''' are continuous on $\mathbf{R}$, and that

$$(u, u', u'', u''') \to (0, 0, 0, 0) \tag{5.3}$$

exponentially fast as $x \to \pm\infty$. Under these assumptions, an application of the Fourier transform to (5.1) is justified and gives

$$\mathrm{F}(u) = \mathrm{F}(w)\mathrm{F}(f(u)). \tag{5.4}$$

An evaluation of $\mathrm{F}(w)$ converts (5.4) to

$$\mathrm{F}(u) = \frac{4b(b^2+1)}{\alpha^4 + 2\alpha^2(b^2-1) + (b^2+1)^2}\mathrm{F}(f(u)). \tag{5.5}$$

Next, multiply both sides of (5.5) by the denominator of $\mathrm{F}(w)$ and use the identities

$$\mathrm{F}(u'''') = \alpha^4\mathrm{F}(u) \quad \text{and} \quad \mathrm{F}(-u'') = \alpha^2\mathrm{F}(u) \tag{5.6}$$

to obtain

$$\mathrm{F}[u'''' - 2(b^2-1)u'' + (b^2+1)^2 u - 4b(b^2+1)f(u)] = 0. \tag{5.7}$$

We claim that (5.7) is satisfied if u is a solution of the problem

$$\begin{cases} u'''' - 2(b^2-1)u'' + (b^2+1)^2 u = 4b(b^2+1)f(u), \\ \lim_{x\to\pm\infty}(u, u', u'', u''') = (0, 0, 0, 0). \end{cases} \tag{5.8}$$

Because $r > 0$, it follows from the definition of $f(u)$ and standard analysis that if u is a solution of (5.8), then u, u', u'', u''', and u'''' are continuous on $\mathbf{R}$, hence (5.7) holds. It then follows that properties (5.4)–(5.7) also hold. From this we conclude that any solution of (5.8) also is a solution of the integral equation (5.1). This reduces the problem of finding N-bump solutions of (5.1) to the study of N-bump solutions of (5.8).

The first goal of our investigation of (5.8) is to extend the results of the previous section where we considered the special case $r = 0$. Thus, we keep $th = 1.5$ and choose an $r > 0$. Our numerical experiments for the case $r = 0$ indicate the existence of even solutions. Thus, when $r > 0$ we will restrict our attention to even solutions of (5.8). These satisfy

$$u'(0) = u'''(0) = 0. \tag{5.9}$$

In the next two sections we use the program AUTO97 [12, 13] to obtain an understanding of the global behavior of families of N-bump solutions of (5.8) as the parameter b varies.

Our second goal is to give global estimates on the range of r, th, and b for which N-bump solutions of (5.8) can exist. We have the following result.

THEOREM 5.1. *Let $r > 0$ and $th > 0$. If there is a value $b > 0$ for which* (5.8) *has a nonconstant solution, then*

$$0 < b \leq \frac{4 + \sqrt{|16 - th^2|}}{th}. \tag{5.10}$$

Remarks. (i) It would be interesting to extend the results of Theorem 5.1 to the special case $r = 0$. When $r = 0$ the function $f(u)$ is discontinuous and the differential equation in (5.8) no longer has a continuous right-hand side. However, since $f(u)$ will now be piecewise constant and the left-hand side of the differential equation is linear, it may be possible to solve (5.8) over restricted domains, piecing together these solutions into a continuous solution for all $x \in (-\infty, \infty)$. We leave this as an open problem.

(ii) The proof of Theorem 5.1 will be postponed until section 10.

(iii) As will be seen in section 6, the upper bound for b in Theorem 5.1 is not particularly tight, but the main purpose of this theorem is to show that there do not exist nonconstant solutions for all positive b.

The differential equation in (5.8) is fourth order, and for $th > 0$ it has a fixed point at the origin. The eigenvalues of the linearization of (5.8) about the origin are $b \pm i$ and $-b \pm i$. Thus, in (u, u', u'', u''') phase space, solutions of (5.8) are homoclinic orbits leading to the bifocus-type fixed point $(u, u', u'', u''') = (0, 0, 0, 0)$ [25]. We note that the differential equation is not generic since the sum of the eigenvalues is zero for all parameter values. This is a simple consequence of the fact that the differential equation in (5.8) is conservative and, in fact, Hamiltonian. This is easily verified, since solutions $u(x)$ satisfy the first integral

$$u'u''' - \frac{(u'')^2}{2} - (b^2 - 1)(u')^2 + (b^2 + 1)^2 Q(u) = 0, \tag{5.11}$$

where $Q(u)$ is defined by

$$Q(u) \equiv \int_0^u \left(s - \left(\frac{8b}{b^2 + 1} \right) e^{-r/(s-th)^2} H(s - th) \right) ds. \tag{5.12}$$

We also note that the differential equation is *reversible* since it contains only even order derivatives.

In recent years, higher order reversible, Hamiltonian equations have played an increasingly important role in modeling pattern formation in physical systems. We mention, for example, the encyclopedic paper by Cross and Hohenberg [11] which describes a wide array of higher order scalar equations. In two recent survey papers, Champneys [5, 6] gives a dynamical systems approach to the analysis of multi-bump, homoclinic orbits in higher order reversible models arising in physics, fluid mechanics, and optics. We also mention the recent book by Peletier and Troy [30] in which methods of analysis of pattern formation in higher order equations are developed from the alternative topological shooting point of view. In the models considered in these works, families of N-bump homoclinic orbits often arise through a Hamiltonian–Hopf

bifurcation from a constant solution. Furthermore, in many of these models the terms involving u are polynomials of degree greater than one. Thus, these terms exhibit *superlinear* growth as $|u| \to \infty$. However, in the model proposed in this paper, the terms involving u exhibit only *linear* growth for large $|u|$. In addition, the rapidly increasing sigmoidal function $f(u)$ given in (3.3) is poorly approximated by polynomials. Finally, as we shall see in the next two sections, our numerical investigation of (5.8) indicates that families of N-bump solutions do not come into existence through a Hamiltonian–Hopf bifurcation from a constant solution. Because of these fundamental differences from other higher order equations, a rigorous proof of existence of N-bump solutions of problem (5.8) should prove to be a challenging problem.

6. Families of N-bump solutions: N odd. In this section we use AUTO97 [12, 13] to determine the global behavior of families of even 1-bump, 3-bump, and 5-bump solutions of the problem

$$\begin{cases} u'''' - 2(b^2-1)u'' + (b^2+1)^2 u = 4b(b^2+1)f(u) \\ \lim_{x\to\pm\infty}(u, u', u'', u''') = (0,0,0,0), \end{cases} \tag{6.1}$$

where

$$f(u) = 2e^{-r/(u-th)^2} H(u-th), \tag{6.2}$$

and $th > 0$, $b > 0$, and $r > 0$ are constants.

In Figure 13 we set $th = 1.5$ and $r = 0.095$, and let b vary, and compute the bifurcation curve for families of even 1-bump and 3-bump solutions of (6.1)–(6.2). The horizontal axis is b and the vertical axis gives the global maximum of u for the corresponding solutions. Figures 14–17 show solutions at specific points $P_0, \ldots, P_7$ on the curve.

Using MATLAB [28], we numerically integrate (3.1)–(3.3) to a steady state, choosing an initial condition which evolves, as $t \to \infty$, into a 1-bump solution at $b = 0.25$. This solution, which we conjecture to be stable, is labeled P_4 on the bifurcation diagram, and is illustrated in the right panel of Figure 16. We then use AUTO97 to continue this solution as b varies. Figure 13 shows 1-bump solutions along the lower branch ${\Gamma_1}^-$ *between* P_1 and P_3. We conjecture that these solutions are unstable. Solutions at P_2 and P_3 are shown in Figure 15. As b decreases along ${\Gamma_1}^-$, solutions cease to be 1-bump solutions at P_1 (the right panel in Figure 14). As b decreases towards zero, solutions acquire arbitrarily many bumps. For example, the point P_0 corresponds to the 3-bump solution shown in the left panel of Figure 14. Note that when $b = 0$, the only bounded even solution of the ordinary differential equation (ODE) in (6.1) is $u(x) = \cos x$, and it is to this that solutions tend as $b \to 0$.

Remark. The first solution in Figure 15 is computed at $b = 0.25$. As $r \to 0^+$, our computations indicate that this solution tends to the 1-bump solution shown in the right panel of Figure 6 in section 4.

Next, we consider the middle branch ${\Gamma_1}^+$ in Figure 13. Along ${\Gamma_1}^+$ we find a second family of 1-bump solutions, some of which we conjecture are stable, *between* P_5 and P_3. As b decreases along ${\Gamma_1}^+$, solutions cease to be 1-bump solutions at P_5 (the left panel in Figure 16). The solution in the right panel of Figure 16 was computed at $b = 0.25$. As $r \to 0^+$, our computations indicate that this solution is stable and tends to the 1-bump solution shown in the left panel of Figure 6 in section 4.

We let ${\Gamma_3}^-$ denote the upper branch of the diagram in Figure 13. Along this branch our computations indicate that solutions are *unstable* 3-bump solutions. Specific solutions at P_6 and P_7 are given in Figure 17. The solution at P_6 is computed

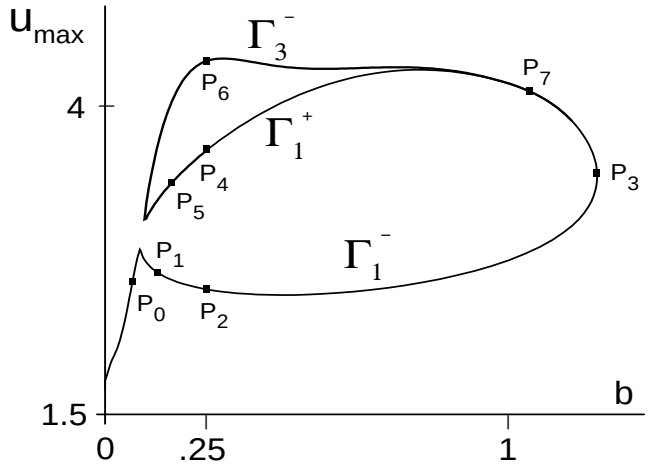

FIG. 13. *Bifurcation curve for* (6.1)–(6.2) *showing* 1*-bump and* 3*-bump solutions. Parameters are* $th = 1.5$ *and* $r = 0.095$. u_{max} *is the maximum of* u *over all* x. *Particular solutions at the points* $P_0, \ldots P_7$ *are shown in Figures* 14–17, *and the labeling of the curves is discussed in the text.*

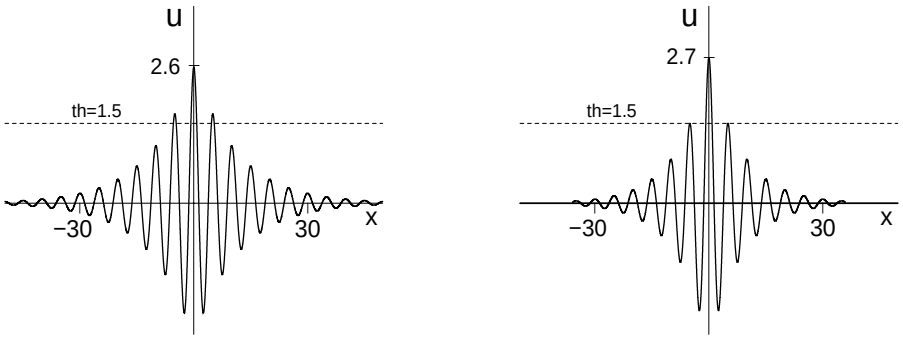

FIG. 14. *Solutions on* $\Gamma_1{}^-$ *at* P_0 *(left) and* P_1 *(right) in Figure* 13.

at $b = 0.25$, and as $r \to 0^+$ our computations indicate that it tends to the solution shown in the right panel of Figure 8.

We have also investigated the existence of 3-bump and 5-bump solutions. Our computations show that these solutions lie on yet another branch leading to the original bifurcation curve in Figure 13. This branch of solutions is labeled $\Gamma_3{}^+$ and $\Gamma_5{}^-$ in Figure 18. In Figure 19 we give specific solutions on $\Gamma_3{}^+$ and $\Gamma_5{}^-$ at $b = 0.25$. Our computations indicate that the solution in the left panel of Figure 19 is stable. Furthermore, as $r \to 0^+$ this solution tends to the solution in the left panel of Figure 8.

We can use data from Figures 13 and 18 to compare the largest values of b for which nonconstant solutions exist with the upper bound given in Theorem 5.1.

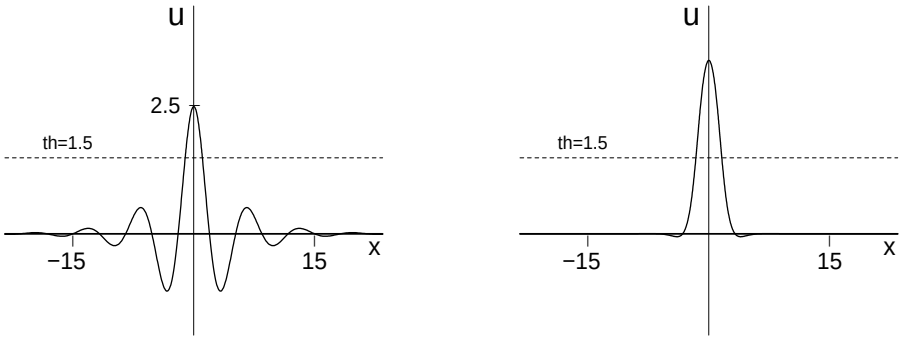

FIG. 15. *Solutions on* $\Gamma_1{}^-$ *at* P_2 *(left) and* P_3 *(right) in Figure* 13.

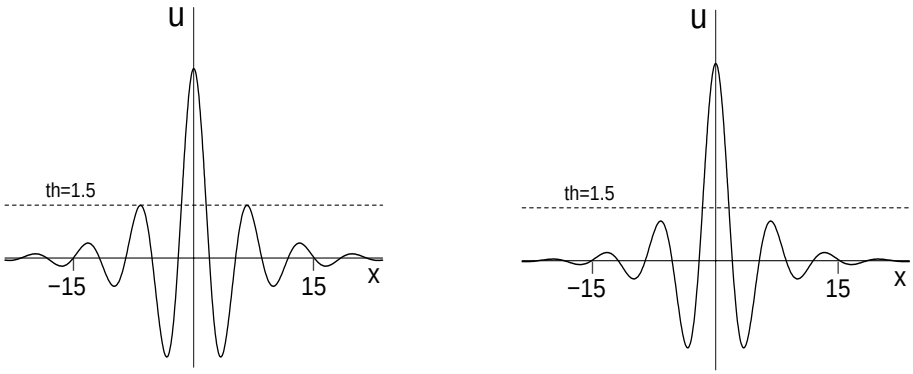

FIG. 16. *Solutions on* $\Gamma_1{}^+$ *at* P_5 *(left) and* P_4 *(right) in Figure* 13.

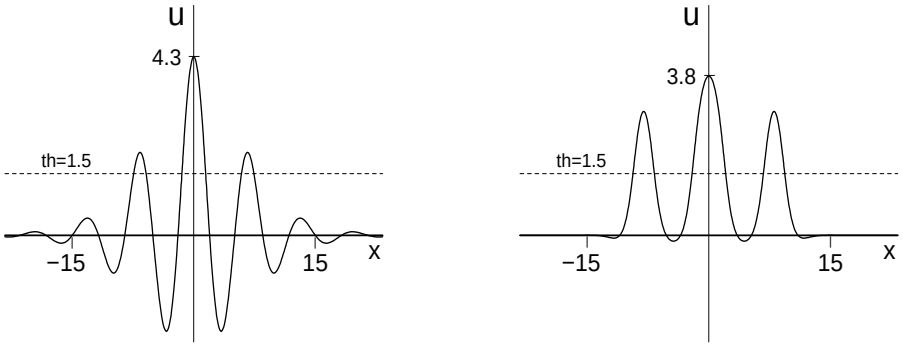

FIG. 17. *Solutions on* $\Gamma_3{}^-$ *at* P_6 *(left) and* P_7 *(right) in Figure* 13.

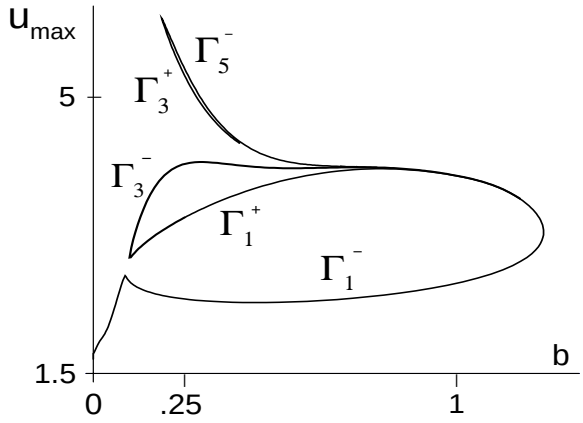

FIG. 18. *Bifurcation curve for* (6.1)–(6.2) *showing* 1, 3, *and* 5*-bump solutions. This Figure is an extension of Figure* 13.

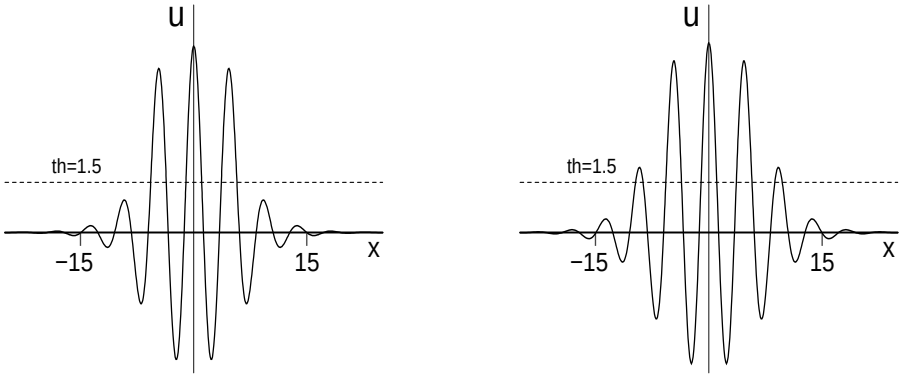

FIG. 19. *Solutions on the curves* $\Gamma_3{}^+$ *(left) and* $\Gamma_5{}^-$ *(right) at* $b = 0.25$ *in Figure* 18.

In Figure 20 we show saddle-node bifurcations of 1-, 3-, and 5-bump solutions in the b, th plane for $r = 0.095$. The curve γ_1 is the continuation of the point P_3 in Figure 13, and the curves γ_3 and γ_5 are the corresponding continuations for 3- and 5-bump homoclinic orbits, respectively. The dashed line (A) is the function given by the equality in (5.10), i.e., the value of b above which Theorem 5.1 states that no nonconstant solutions of (6.1)–(6.2) can exist. We see that the solutions studied in this section are compatible with Theorem 5.1, but that the bound given there is not particularly tight.

We have done one further experiment which shows how quickly the global behavior of solutions can change. In Figures 13 and 18 we set $th = 1.5$ and $r = 0.095$ and found that two "cusps" form on the left side of the bifurcation diagram. In Figure 21 we have increased r from $r = 0.095$ to $r = 0.1$ and repeated our computations. In

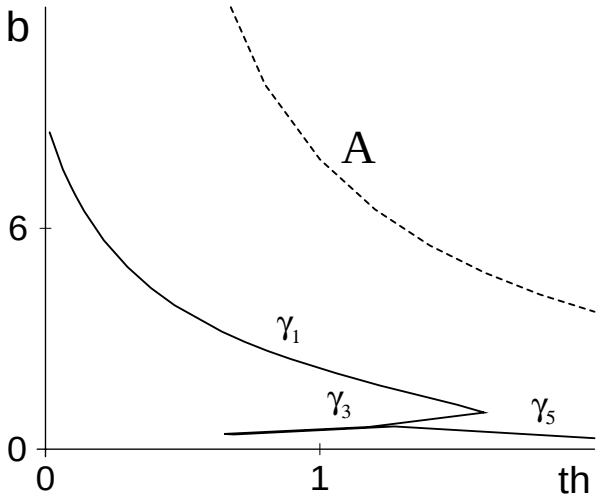

FIG. 20. *The continuation of the saddle-node bifurcations marking the largest values of b for which various orbits exist, compared with the upper bound given in Theorem* 5.1. γ_1 *is the continuation of the point* P_3 *in Figure* 13, *while* γ_3 *and* γ_5 *are continuations of the corresponding points for* 3- *and* 5-*bump homoclinic orbits. The curve "A" is the function* $b = (4+\sqrt{|16-th^2|})/th$, *given in* (5.10).

this case we find that the cusps have now joined and the 1-bumps solutions lie on an isolated closed curve. The lower branch Γ_1^- consists of small amplitude 1-bump solutions, which are conjectured to be unstable. The upper branch Γ_1^+ consists of large amplitude 1-bump solutions, some of which are conjectured to be stable. In order to see the separation of curves more clearly, in Figure 22 we have redrawn the bifurcation diagram of Figure 21 but now we have replaced u_{max} on the vertical axis with the L^2 norm of the solution (the default L^2 norm of AUTO97 is used). Figure 22 suggests that a "snaking" phenomenon occurs in the branches of the bifurcation curve and that solutions acquire more bumps as the L^2 norm increases (e.g., see Figure 23). Similar snaking phenomena occur in other physical systems modeled by higher order scalar equations [21, 30, 38], as well as in systems where homoclinic orbits are present [20].

7. Families of *N*-bump solutions: *N* even. In this section we determine the global behavior of families of 2-bump, 4-bump, and 6-bump solutions of the problem

$$\begin{cases} u'''' - 2(b^2-1)u'' + (b^2+1)^2 u = 4b(b^2+1)f(u), \\ \lim_{x\to\pm\infty}(u,u',u'',u''') = (0,0,0,0), \end{cases} \tag{7.1}$$

where

$$f(u) = 2e^{-r/(u-th)^2}H(u-th). \tag{7.2}$$

Here $H(\cdot)$ is the Heaviside function, $th > 0$ is the threshold, and $b > 0$, $r > 0$ are constants.

In Figure 24 we again keep $th = 1.5$ and $r = 0.095$, and let b vary, and compute the bifurcation curve for families of even 2-bump and 4-bump solutions of (7.1)–(7.2).

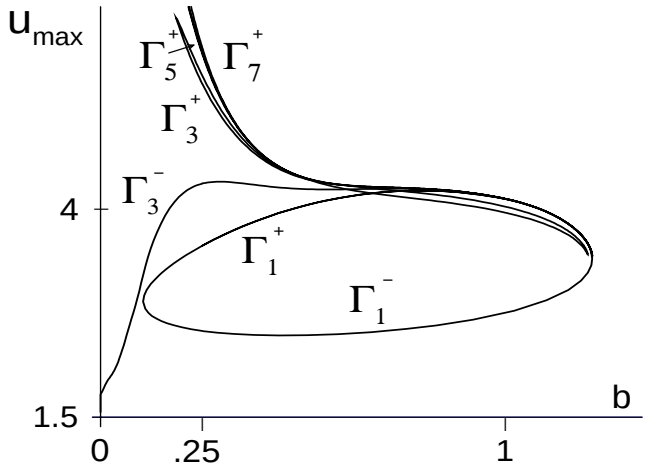

FIG. 21. *Bifurcation curve for* (6.1)–(6.2) *showing* 1-, 3-, 5-, *and* 7-*bump solutions. Parameters are* $th = 1.5$ *and* $r = 0.1$. *Compare this with Figure* 18.

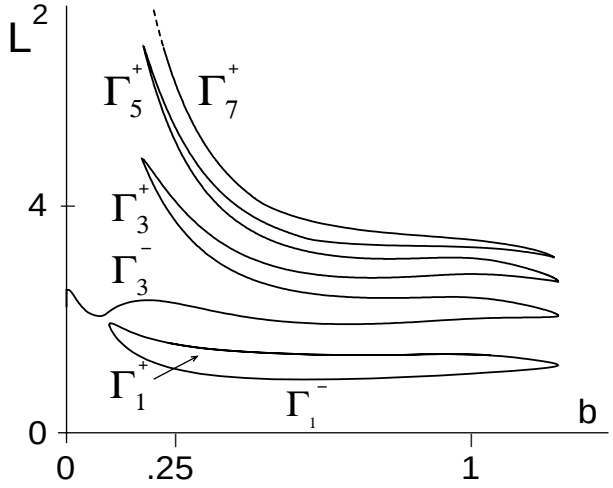

FIG. 22. *The same curves as in Figure* 21*, but the vertical axis is now the* L^2 *norm of the solutions.*

Figures 25–28 show solutions at specific points $P_0, \ldots, P_7$ on this curve. To compute the curve in Figure 24 we first set $b = 0.25$ and integrate (3.1)–(3.3) with an initial condition chosen so that the solution converges, as $t \to \infty$, to the 2-bump (apparently stable) solution indicated by point P_4, and illustrated in the right panel of Figure 27. We then use AUTO97 to continue this solution as b varies. In Figure 24 we find 2-bump solutions, which are conjectured to be unstable, along the lower branch $\Gamma_2{}^-$

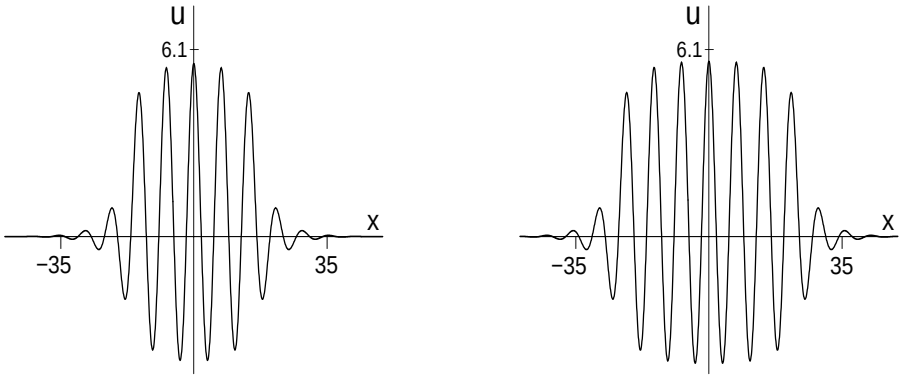

FIG. 23. *Solutions on the curves* Γ_5^+ *(left) and* Γ_7^+ *(right) in Figure* 22. *Parameters are* $r = 0.1$, $th = 1.5$, and $b = 0.25$.

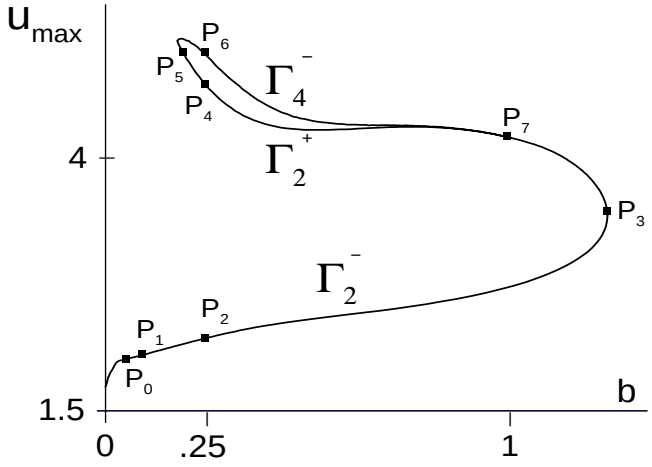

FIG. 24. *Bifurcation curve of* 2*-bump and* 4*-bump solutions for* (7.1)–(7.2). *Solutions at the points* $P_0, \ldots, P_7$ *are shown in Figures* 25–28. *Parameters are* $r = 0.095$, $th = 1.5$. *Compare with Figure* 13.

between P_1 ($b = 0.045$) and P_3 ($b = 1.23$). Solutions at P_2 ($b = 0.25$) and P_3 are shown in Figure 26. As b decreases along $\Gamma_2{}^-$, solutions cease to be 2-bump solutions at P_1 (right panel in Figure 25). To the left of P_1 our computations imply that solutions acquire arbitrarily many bumps as $b \to 0^+$, as was the case for bumps with N odd. For example, at $b = 0.03$ the point P_0 corresponds to the 4-bump solution in the left panel of Figure 25.

Remark. The solution in the left panel of Figure 26 is computed at $b = 0.25$. As $r \to 0^+$, our computations indicate that this solution is unstable and tends to the 2-bump solution shown in the right panel of Figure 7.

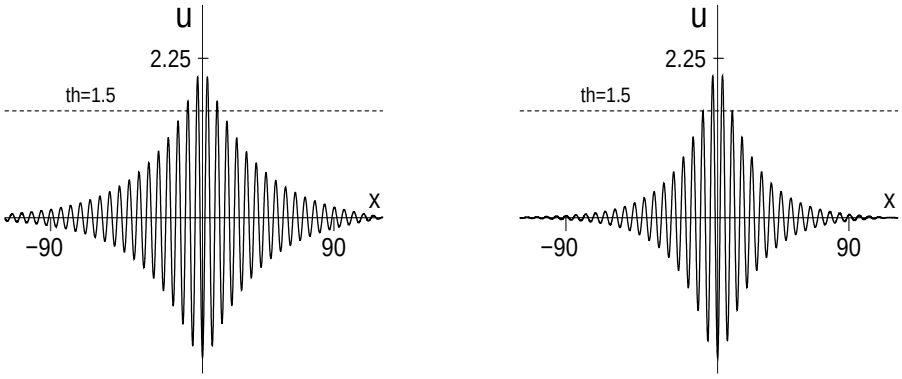

FIG. 25. *Solutions on* $\Gamma_2{}^-$ *at* P_0 *(left) and* P_1 *(right) in Figure* 24.

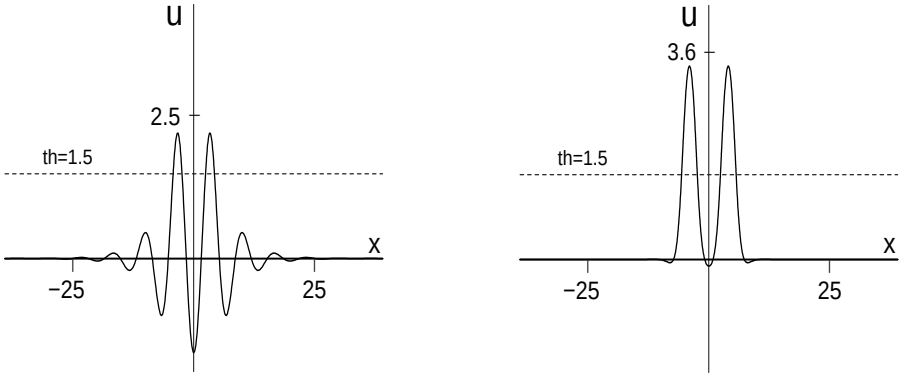

FIG. 26. *Solutions on* $\Gamma_2{}^-$ *at* P_2 *(left) and* P_3 *(right) in Figure* 24.

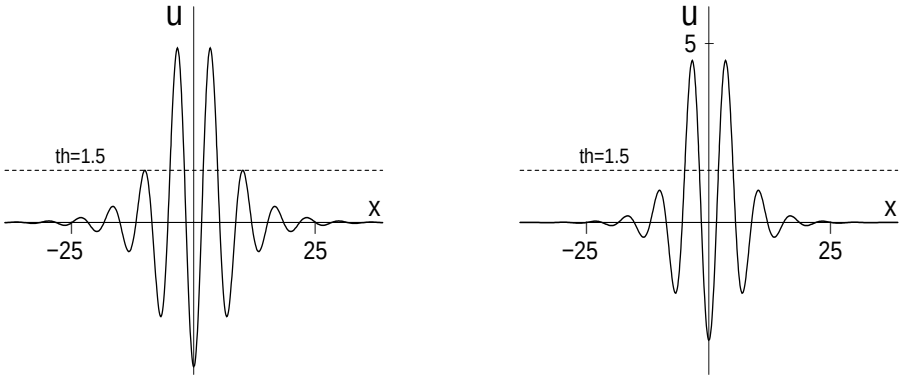

FIG. 27. *Solutions on* $\Gamma_2{}^+$ *at* P_5 *(left) and* P_4 *(right) in Figure* 24.

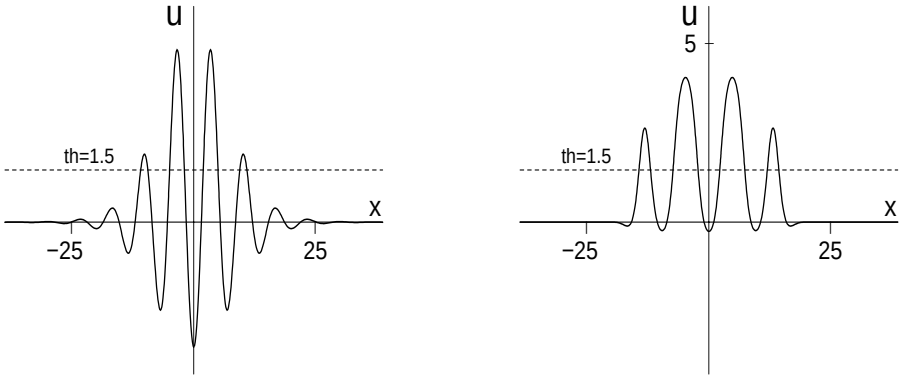

FIG. 28. *Solutions on* $\Gamma_4{}^-$ *at* P_6 *(left) and* P_7 *(right) in Figure* 24.

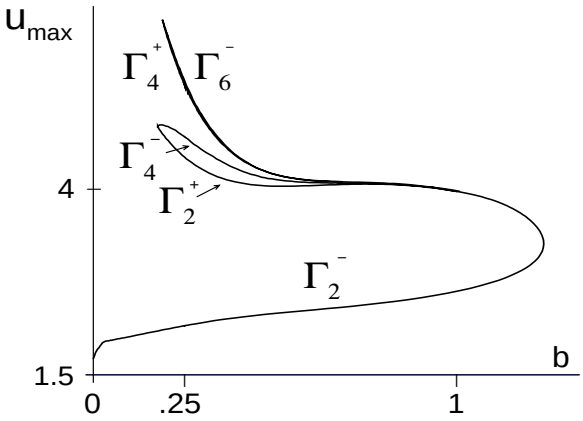

FIG. 29. *Bifurcation curve for* 2, 4, *and* 6*-bump solutions of* (7.1)–(7.2). *This figure is an extension of Figure* 24.

Next, along the middle branch $\Gamma_2{}^+$ in Figure 24 we find a family of 2-bump solutions, some of which are conjectured to be stable, between P_5 ($b = 0.187$) and P_3 ($b = 1.23$). As b decreases along $\Gamma_2{}^+$, solutions cease to be 2-bump solutions at P_5 (shown in the left panel of Figure 27). The solution in the right panel of Figure 27 corresponds to P_4 ($b = 0.25$) in Figure 24. As $r \to 0^+$ this solution tends to the 2-bump solution shown in the left panel of Figure 7.

We let $\Gamma_4{}^-$ denote the upper branch in Figure 24. Along this branch our computations indicate that solutions are *unstable* 4-bump solutions. The solutions at P_6 ($b = 0.25$) and P_7 ($b = 0.99$) are shown in Figure 28. We have also found another family of 4-bump solutions, as well as 6-bump solutions. These solutions lie on a second branch leading to the original curve in Figure 24. The lower and upper curves on this branch are given by $\Gamma_4{}^+$ and $\Gamma_6{}^-$ in Figure 29. In Figure 30 we give specific solutions on $\Gamma_4{}^+$ and $\Gamma_6{}^-$ at $b = 0.25$. Our computations indicate that the solution in the left panel of Figure 30 is stable and tends to the solution in the left panel of Figure 9 as $r \to 0^+$.

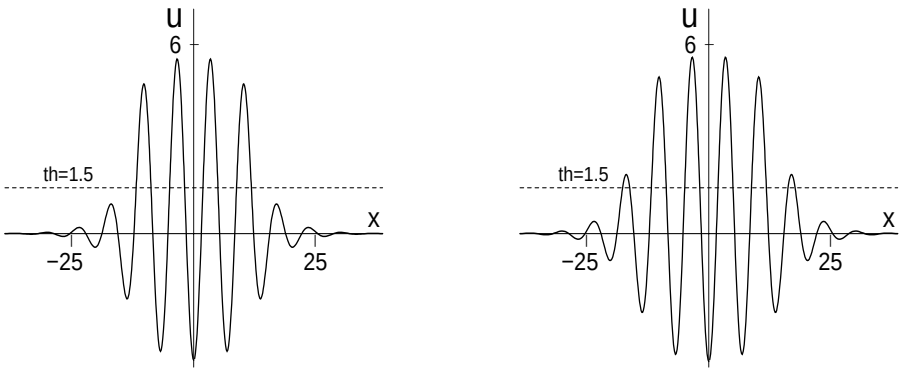

FIG. 30. *Solutions on* $\Gamma_4{}^+$ *(left) and* $\Gamma_6{}^-$ *(right) at* $b = 0.25$ *in Figure* 29.

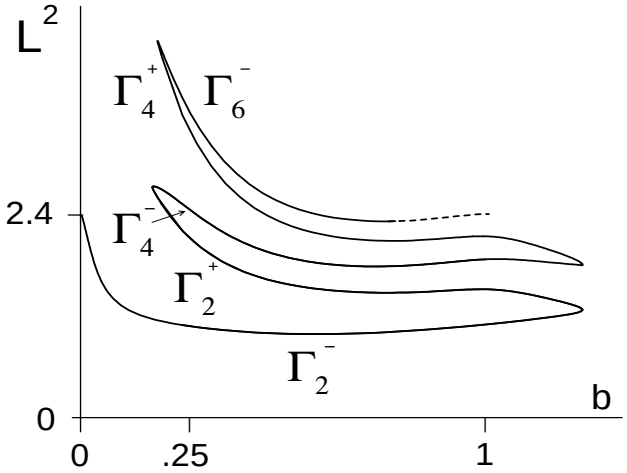

FIG. 31. *The same curves as in Figure* 29, *but the vertical axis is now the* L^2 *norm of the solutions.*

As in the previous section, we redraw in Figure 31 the bifurcation curve shown in Figure 29 but using the L^2 norm for the vertical axis. This allows us to see the separation of branches and, once again, a snaking diagram results.

While we have only looked at multi-bump solutions for which successive maxima of u monotonically increase and then decrease as a function of x, there may also exist "$(n + m)$-bumps" for integer $n, m \geq 1$. These would have the approximate form of an n-bump "glued" to an m-bump, with sufficient low-amplitude oscillations between them. The linearization of (5.8) about the origin has the form necessary for these "composite" orbits to exist, and to confirm this conjecture one would need to check that the N-bump orbits studied above were formed by transverse intersections of the stable and unstable manifolds of the origin (a generic property). See [7] and references

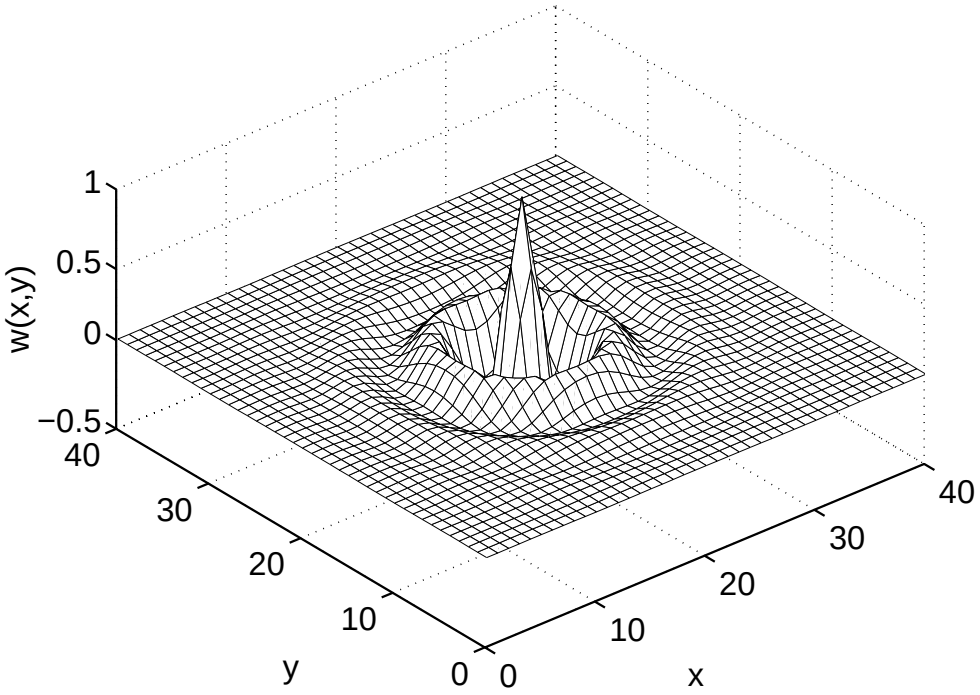

FIG. 32. *Coupling function $w(x, y)$, (8.2), for $b = 0.3$, centered at the center of the domain.*

therein for more details.

8. Extension to two space dimensions. In this section we extend our model to include two spatial dimensions. The system we study, an analogy of (3.1)–(3.3), is the following:

$$\frac{\partial u(x,y,t)}{\partial t} = -u(x,y,t) + \iint_{\Omega} w(x-q, y-s) f(u(q,s,t))\, dq\, ds, \tag{8.1}$$

where

$$w(x,y) = e^{-b\sqrt{x^2+y^2}} \left(b \sin\left(\sqrt{x^2+y^2}\right) + \cos\left(\sqrt{x^2+y^2}\right)\right), \tag{8.2}$$

and

$$f(u) = 2e^{-r/(u-th)^2} H(u-th). \tag{8.3}$$

The coupling function (8.2) is the same as (3.2), with distance in one dimension now replaced by distance in two dimensions. An example is shown in Figure 32. The rate function, (8.3), is identical to (3.3).

A typical stable solution of (8.1)–(8.3) is shown in Figure 33 for the parameters $r = 0.1$, $th = 1.5$, and $b = 0.45$. The initial condition was $u(x, y, 0) = 5$ for $16 < x < 25.6$ and $8 < y < 24$, and $u(x, y, 0) = 0$ otherwise. The domain, Ω, is a square of side-length 40, discretized by a regular 50×50 grid, with open boundaries; i.e., there are no constraints on u or any of its derivatives at the boundaries, and the integral

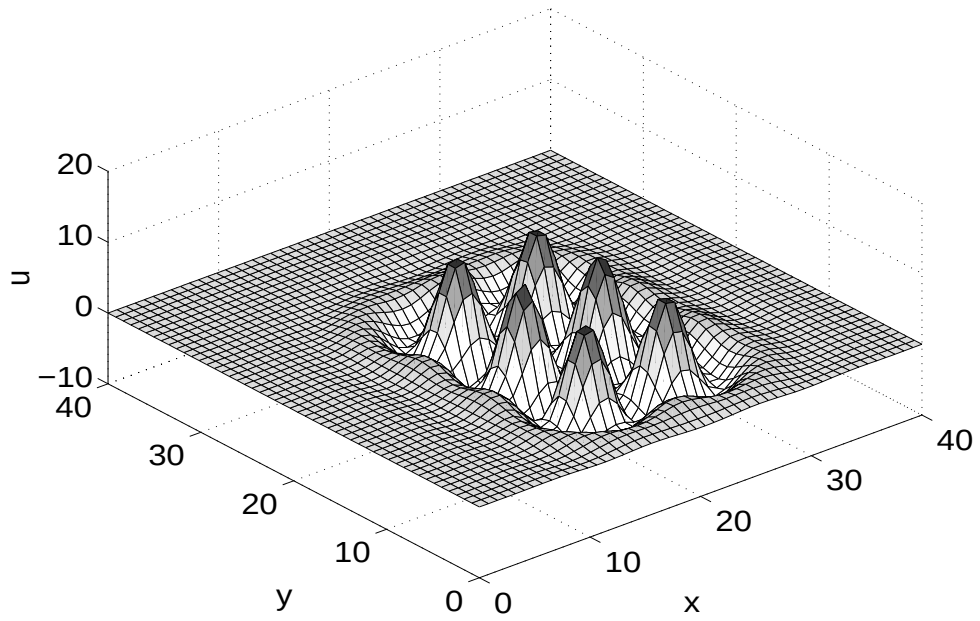

FIG. 33. *A "6-bump" stable solution of* (8.1)–(8.3). *Parameters are* $b = 0.45$, $r = 0.1$, $th = 1.5$.

in (8.1) is taken over only Ω. Note that while the coupling function (8.2) is radially symmetric, the domain is not, and so we do not expect the resulting solutions to have radial symmetry. The equation (8.1) was integrated using an Euler step until the solution converged to a steady state, and at each time step the double integral was approximated by a Riemann integral using the values of u on the grid mentioned above. Note that the convolution can be performed more efficiently by using the two-dimensional fast Fourier transform.

Figure 33 shows the resultant 6-bump solution, and the distance between local maxima is approximately the same as the distance between successive maxima of the coupling function (2π). The regularity is a reflection of the initial condition; more irregular initial conditions lead to an irregular cluster of bumps with similar spacing between local maxima (not shown). That is, keeping $r = 0.1$, $th = 1.5$, and $b = 0.45$, it is possible to find other stable clusters with small numbers of bumps, with the exact number and position being determined by the initial condition. This is analogous with the one-dimensional model (3.1)–(3.3) where stable multi-bump solutions coexist for $b = 0.25$ (see Figure 19 (left), Figure 23, Figure 27 (right), and Figure 30 (left)). In the two-dimensional model, as b is decreased from $b = 0.45$ it seems more difficult to find localized clusters of multi-bump solutions. Instead, for smaller b, either an initial set of u values will die down to $u = 0$ if b is too small or else the entire domain will be filled with bumps. An example with $b = 0.3$ and the other parameters the same (i.e., $r = 0.1$ and $th = 1.5$) is shown in Figure 34. This "progressive recruitment" phenomenon is the same as that seen by Gutkin, Ermentrout, and O'Sullivan in a one-dimensional model [16]. Similar patterns were also found by Usher, Stemmler, and Olami [34] in a neural model with short-range excitation and long-range inhibition.

For larger b, stable attractors also form, but they do not seem to retain the structure of a cluster of bumps observed in Figure 33. However, there still appears

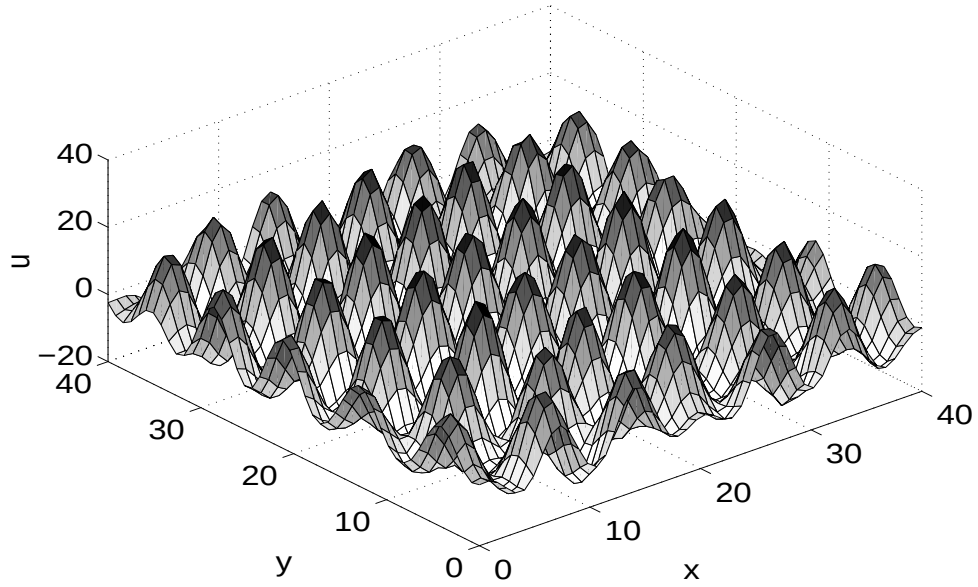

FIG. 34. *A stable solution of* (8.1)–(8.3). *Parameters are* $b = 0.3$, $r = 0.1$, $th = 1.5$. *The initial* u *was spatially localized.*

to be a characteristic length similar to the interbump spacing seen for lower b. In Figure 35, keeping $r = 0.1$ and $th = 1.5$, we increase b to $b = 0.7$ and illustrate an example of this type of stable attractor. For still larger b values, the whole domain becomes active and there are no structures with characteristic length 2π. This is probably due to the lack of a significant inhibitory component to w when b is large—see Figure 4, right panel, for an illustration of this effect in the one-dimensional setting.

In this section, we have presented only numerical results. We leave the possible derivation of a differential equation problem whose solutions describe steady states of (8.1)–(8.3), and any further analysis, as open problems. Although few mathematical results exist for two-dimensional neural models, some interesting results have been obtained relating to the study of circular stationary solutions [2, 31, 36].

9. Proof of Theorem 2.1. In this section we prove Theorem 2.1 concerning the nonexistence of a class of 2-bump solutions of problem (2.2)–(2.3). Recall from section 2 that $u(x)$ is a 2-bump solution of (2.2)–(2.3) if there are values $0 < a < b < c$ such that

$$\begin{cases} u > 0 \quad \text{on} \quad (0,a) \cup (b,c), \\ u(0) = u(a) = u(b) = u(c) = 0, \\ u < 0 \quad \text{otherwise.} \end{cases} \tag{9.1}$$

We define the "distance between bumps" to be $b - a$. Also, we recall from section 2 that under hypotheses (H_1)–(H_6), the function $w(x)$ is symmetric with respect to $x = 0$, that $w(x)$ attains a unique local minimum on $\mathbf{R}^+$ at a value $x_0 > 0$, and that $w(x)$ is *increasing* on (x_0, ∞) (see Figure 1). We will use these properties in our proof of the following result (a restatement of Theorem 2.1).

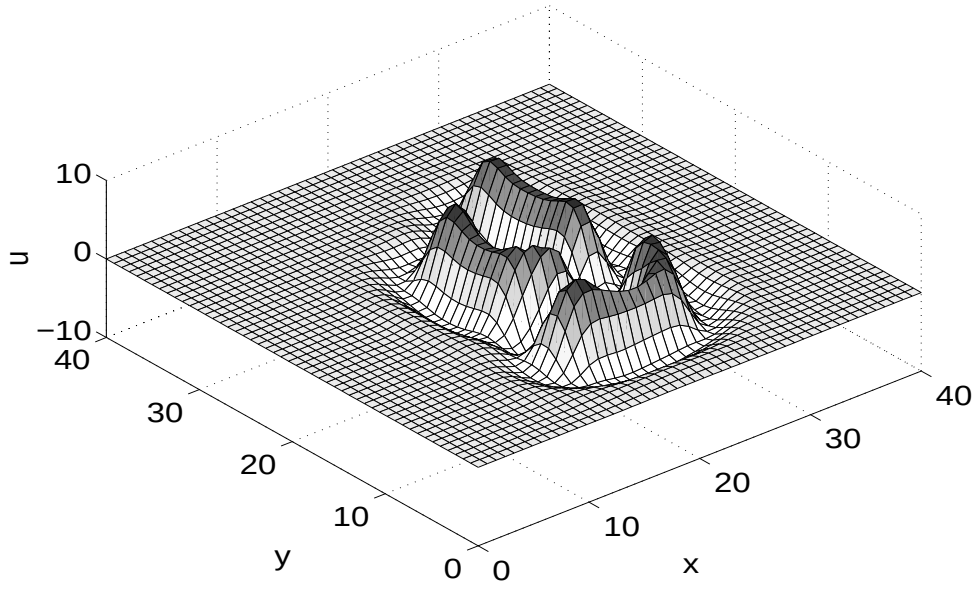

FIG. 35. *A stable solution of* (8.1)–(8.3). *Parameters are* $b = 0.7$, $r = 0.1$, $th = 1.5$. *The initial condition was random but spatially localized.*

THEOREM 9.1. *Under hypotheses* (H_1)–(H_6) *there is no value* $h \in \mathbf{R}$ *for which the problem* (2.2)–(2.3) *has a* 2*-bump solution satisfying* (2.9) *such that the distance between bumps satisfies* $b - a \geq x_0$.

Proof. We assume that there is an $h \in \mathbf{R}$ for which (2.2)–(2.3) has a solution satisfying (2.9), with $b - a \geq x_0$. Using (H_1)–(H_6), we will obtain a contradiction of this assumption. From (2.2), (2.3) and (2.9), it follows that $u(x)$ can be written in the form

$$u(x) = \int_0^a w(x-y)\,dy + \int_b^c w(x-y)\,dy + h \qquad \forall x \in \mathbf{R}. \tag{9.2}$$

Next, recall from (2.4) that $W(x)$ is defined by

$$W(x) = \int_0^x w(y)\,dy \qquad \forall x \in \mathbf{R}. \tag{9.3}$$

Hypotheses (H_1)–(H_6) imply that $W(x)$ is odd. That is,

$$W(x) = -W(-x) \qquad \forall x \in \mathbf{R}. \tag{9.4}$$

Using (9.3), we write (9.2) as

$$u(x) = W(x) - W(x-a) + W(x-b) - W(x-c) + h. \tag{9.5}$$

Because $u(b) = u(c) = W(0) = 0$, it follows from (9.5) that

$$u(c) = W(c) - W(c-a) + W(c-b) + h = 0, \tag{9.6}$$

and

$$u(b) = W(b) - W(b-a) - W(b-c) + h = 0. \tag{9.7}$$

We note that $W(c-b) = -W(b-c)$ since $W(x)$ is odd. Thus, a subtraction of (9.7) from (9.6) leads to

$$W(c) - W(b) = W(c-a) - W(b-a). \tag{9.8}$$

Recalling the definition of $W(x)$ from (9.3), we write (9.8) as

$$\int_b^c w(y)dy = \int_{b-a}^{c-a} w(y)dy. \tag{9.9}$$

Also, our hypothesis that $b - a \geq x_0$ implies that

$$x_0 \leq b - a < c - a. \tag{9.10}$$

We need to consider two cases to complete the proof. The first case is

$$x_0 \leq b - a < c - a \leq b < c. \tag{9.11}$$

From (H_6) and (9.10) we conclude that $w(x)$ is increasing on $(b-a, c)$. Thus, $w(x) > w(b)$ on (b, c), and $w(x) < w(c-a)$ on $(b-a, c-a)$. This implies that

$$\int_b^c w(y)dy > w(b)(c-b), \tag{9.12}$$

and

$$\int_{b-a}^{c-a} w(y)dy < w(c-a)(c-b). \tag{9.13}$$

Combining (9.9), (9.11), (9.12), and (9.13), we conclude that

$$w(b) < w(c-a). \tag{9.14}$$

However, since (H_6) implies that $w(x)$ is nondecreasing on $[c-a, b]$, it follows that $w(b) \geq w(c-a)$, contradicting (9.14). The second case we need to consider is

$$x_0 \leq b - a < b < c - a < c. \tag{9.15}$$

Then (9.9) can be written as

$$\int_b^{c-a} w(y)dy + \int_{c-a}^{c} w(y)dy = \int_{b-a}^{b} w(y)dy + \int_b^{c-a} w(y)dy.$$

This reduces to

$$\int_{c-a}^{c} w(y)dy = \int_{b-a}^{b} w(y)dy. \tag{9.16}$$

Again, we use the fact that $w(x)$ is increasing on (x_0, c), together with (9.15), and conclude that

$$\int_{c-a}^{c} w(y)dy > w(c-a)a \tag{9.17}$$

and

$$\int_{b-a}^{b} w(y)dy < w(b)a. \tag{9.18}$$

From (9.16)–(9.18) it follows that $w(b) > w(c-a)$. However, this is a contradiction since $w(x)$ increases on $(b, c-a)$. The proof of Theorem 2.1 is now complete.

10. Proof of Theorem 5.1. In this section we prove Theorem 5.1 and determine a global parameter regime over which nonconstant solutions of the problem

$$\begin{cases} u'''' - 2(b^2-1)u'' + (b^2+1)^2 u = 4b(b^2+1)f(u), \\ \lim_{x\to\pm\infty}(u,u',u'',u''') = (0,0,0,0) \end{cases} \tag{10.1}$$

might possibly exist. We recall that $f(u)$ is defined by

$$f(u) = 2e^{-r/(u-th)^2}H(u-th), \tag{10.2}$$

where $H(u-th)$ is the Heaviside function (see Figure 5). For convenience we restate our result (Theorem 5.1) below.

THEOREM 10.1. *Let $r > 0$ and $th > 0$. If there is a value $b > 0$ for which (10.1)–(10.2) has a nonconstant solution, then*

$$0 < b \le \frac{4+\sqrt{|16-th^2|}}{th}.$$

Proof. Suppose that $u(x)$ is a nonconstant solution of (10.1)–(10.2) for some

$$r > 0,\ th > 0, \quad \text{and} \quad b > \frac{4+\sqrt{|16-th^2|}}{th}. \tag{10.3}$$

We will obtain a contradiction of this assumption. First, we observe that

$$\frac{4+\sqrt{|16-th^2|}}{th} \ge 1 \qquad \forall\ th > 0. \tag{10.4}$$

It then follows from (10.3) and (10.4) that $b > 1$. Next, from (10.1)–(10.2) it is easily verified that $u(x)$ must satisfy the first integral

$$u'u''' - \frac{(u'')^2}{2} - (b^2-1)(u')^2 + (b^2+1)^2 Q(u) = 0, \tag{10.5}$$

where $Q(u)$ is defined by

$$Q(u) \equiv \int_0^u \left(s - \left(\frac{8b}{b^2+1}\right) e^{-r/(s-th)^2} H(s-th) \right) ds. \tag{10.6}$$

Over the range given in (10.3), we claim that the integrand in (10.6) satisfies

$$u - \left(\frac{8b}{b^2+1}\right) e^{-r/(u-th)^2} H(u-th) > 0 \qquad \forall u > 0. \tag{10.7}$$

First, suppose that $0 < u \le th$. Then $f(u) = 0$ by (10.2), and therefore the left side of (10.7) must be positive. If $u > th$, then

$$u - \left(\frac{8b}{b^2+1}\right) e^{-r/(u-th)^2} H(u-th) > th - \frac{8b}{b^2+1} > 0,$$

since we assume that $th > 0$, $r > 0$, and $b > (4+\sqrt{|16-th^2|})/th$. Thus (10.7) is proved. From (10.6) and (10.7) we conclude that $Q(0) = 0$,

$$Q(u) > 0 \quad \text{if} \quad |u| > 0, \qquad \lim_{|u|\to\infty} Q(u) = \infty, \tag{10.8}$$

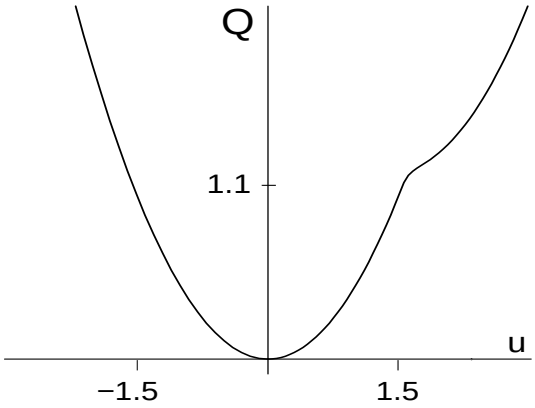

FIG. 36. $Q(u)$, (10.6), *for parameter values* $r = 0.005,\ th = 1.5,\ b = 5.2$.

and

$$\frac{dQ}{du} < 0 \qquad \forall u < 0, \qquad \frac{dQ}{du} > 0 \qquad \forall u > 0. \tag{10.9}$$

For example, the parameters $r = 0.005$, $th = 1.5$, and $b = 5.2$ satisfy (10.3), and in Figure 36 we graph the corresponding $Q(u)$.

Next, because (10.1)–(10.2) is autonomous, we may assume that the solution $u(x)$ attains its global maximum at $x = 0$. We claim that $u(0) > th$. If, on the contrary, $u(0) \le th$, then $u(x) \le th$ for all $x \in \mathbf{R}$, and it follows from (10.2) that $f(u) = 0$ for all $x \in \mathbf{R}$. This reduces the integral equation (5.1) to $u(x) = 0$, and we arrive at a contradiction since we assume that $u(x)$ is a *nonconstant* solution of (10.1)–(10.2), and solutions of (10.1)–(10.2) also are solutions of (5.1). Thus, at $x = 0$ it must be the case that

$$u(0) > th,\ u'(0) = 0, \quad \text{and} \quad u''(0) \le 0. \tag{10.10}$$

Substituting (10.10) into (10.5), and using (10.8), we conclude that

$$u''(0) = -(b^2 + 1)\sqrt{2Q(u(0))} < 0. \tag{10.11}$$

Without loss of generality we may assume that $u'''(0) \le 0$. Otherwise, if $u'''(0) > 0$, then it would suffice to consider the function $v(x) = u(-x)$ which also is a solution of (10.1)–(10.2) and satisfies the initial conditions

$$v(0) > th,\ v'(0) = 0,\ v''(0) < 0, \quad \text{and} \quad v'''(0) < 0.$$

Thus, it may be assumed that the solution $u(x)$ satisfies

$$u(0) > th,\ u'(0) = 0,\ u''(0) < 0, \quad \text{and} \quad u'''(0) \le 0. \tag{10.12}$$

Our goal in the remainder of the proof is to show that there is an $\bar{x} > 0$ such that $u(\bar{x}) > u(0)$. This will contradict the fact that $u(x)$ attains its global maximum

at $x = 0$. Thus, we need to follow the solution as x increases from $x = 0$. Throughout we will make extensive use of the first integral (10.5) and the associated functional $Q(u(x))$. In Figures 37 and 38 we follow $u(x)$ and $Q(u(x))$, respectively, and keep track of the points where the solution $u(x)$ attains its maxima and minima.

From (10.1)–(10.4), (10.7), and (10.12) it follows that $u''''(0) < 0$. This and (10.12) imply that $u'''(x) < 0$ on an interval $(0, \epsilon)$. We set

$$\sigma = \sup\{\hat{x} > 0 | u'''(x) < 0 \quad \forall x \in (0, \hat{x})\}. \tag{10.13}$$

If $\sigma = \infty$, then $u''(x) < u''(0) < 0$ for all $x > 0$, hence $u''(\infty) < 0$, contradicting the condition $u''(\infty) = 0$ given in (10.1). Thus, it must be the case that $\sigma < \infty$, $u'''(\sigma) = 0$, and

$$u(x) < u(0),\ u'(x) < 0, \quad \text{and} \quad u''(x) < u''(0) < 0 \qquad \forall x \in (0, \sigma]. \tag{10.14}$$

Next, it follows from (10.8) and (10.9) that there is a unique, negative value $u_1 < 0$ (see Figure 38) such that

$$Q(u) < Q(u(0)) \qquad \forall u \in (u_1, u(0)), \quad \text{and} \quad Q(u_1) = Q(u(0)). \tag{10.15}$$

We need to show that $u(\sigma) < u_1$. If $u(\sigma) \geq u_1$, then from (10.11), (10.14), and (10.15) it follows that $(u'')^2$ *increases* on $(0, \sigma)$ so that

$$\frac{(u(x)'')^2}{2} > (b^2 + 1)^2 Q(u(x)) \qquad \forall x \in (0, \sigma]. \tag{10.16}$$

Setting $x = \sigma$ in (10.5), and using (10.3), (10.4), (10.14), and (10.16), we obtain

$$-(u'(\sigma))^2(b^2 - 1) > 0,$$

a contradiction since $u'(\sigma) < 0$ and $b > 1$. Therefore it must be the case that $u(\sigma) < u_1$. Thus, there is an $x_1 \in (0, \sigma)$ such that (see Figure 37)

$$u'(x) < 0,\ u''(x) < 0,\ u'''(x) < 0 \qquad \forall x \in (0, x_1], \quad \text{and} \quad u(x_1) = u_1. \tag{10.17}$$

Since $u(\infty) = 0$, it follows from (10.17) that there is an $x_2 > x_1$ such that

$$u'(x) < 0 \qquad \forall x \in [x_1, x_2), \quad \text{and} \quad u'(x_2) = 0. \tag{10.18}$$

We conclude from (10.5) and (10.18) that

$$u(x_2) < u_1 < 0,\ u'(x_2) = 0, \text{ and } u''(x_2) = (b^2 + 1)\sqrt{2Q(u(x_2))} > 0. \tag{10.19}$$

We need to determine the sign of $u'''(x_2)$. Because $u''(x_1) < 0$ and $u''(x_2) > 0$, there is an $\tilde{x} \in (x_1, x_2)$ where $u''(\tilde{x}) = 0$ and $u'''(\tilde{x}) \geq 0$. This, (10.3), (10.4), and (10.18) give

$$u'''(\tilde{x}) - 2(b^2 - 1)u'(\tilde{x}) > 0. \tag{10.20}$$

Next, because $u(x) < u_1 < 0$ on $[\tilde{x}, x_2]$, it follows from (10.1)–(10.2) that

$$(u''' - 2(b^2 - 1)u')' = -(b^2 + 1)^2 u > 0 \qquad \forall x \in [\tilde{x}, x_2]. \tag{10.21}$$

From (10.19), (10.20), and (10.21) we conclude that

$$u'''(x_2) > 0. \tag{10.22}$$

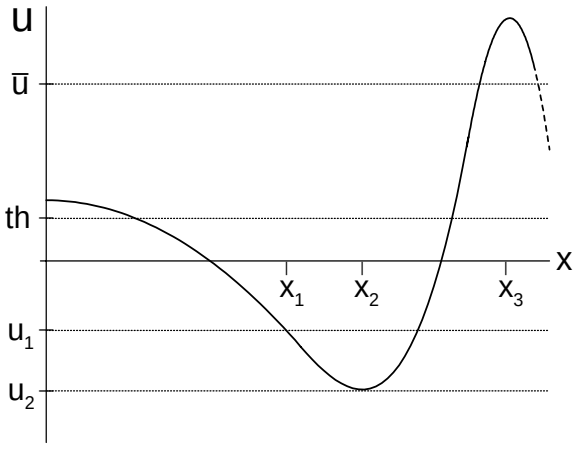

FIG. 37. *A sketch of* $u(x)$ *for* (10.1)–(10.2): $u(x_1) = u_1,\ u(x_2) = u_2$, *and* $u(x_3) > \bar{u}$.

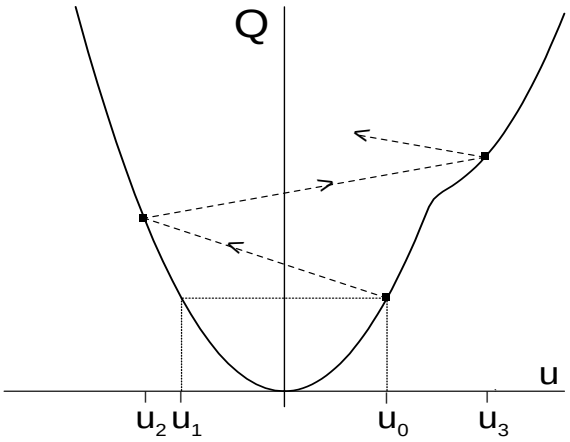

FIG. 38. $Q(u)$, (10.6): $u_0 = u(0),\ u_1 = u(x_1) = u_0,\ u_2 = u(x_2),\ u_3 = u(x_3)$.

In Figure 38 we set $u_1 = u(x_1)$ and $u_2 = u(x_2)$. As $u(x)$ decreases from u_1 to u_2, properties (10.8) and (10.9) imply that $Q(u)$ *increases*, and therefore

$$Q(u(x_2)) > Q(u_1) = Q(u(0)). \tag{10.23}$$

In the final step of the proof we follow $u(x)$ as x increases from $x = x_2$, and we show that there is an $x_3 > x_2$ such that $u(x_3) = u_3 > u(0)$ (see Figures 37 and 38). We first observe from (10.8)–(10.9) that there is a unique $\bar{u} > 0$ such that $Q(\bar{u}) = Q(u(x_2))$.

It follows from (10.23), and the fact that $Q(u)$ is increasing for $u > 0$, that

$$\bar{u} > u(0). \tag{10.24}$$

Next, define

$$x_3 = \sup\{\hat{x} > x_2 | u'''(x) > 0 \ \forall x \in (x_2, \hat{x})\}. \tag{10.25}$$

Because of (10.24), if we show that $u(x_3) > \bar{u}$, we will obtain a contradiction of the fact that $u(x)$ has its global maximum at $x = 0$. From (10.19), (10.22), and (10.25) it follows that

$$u'(x) > 0, \quad u''(x) > u''(x_2) = (b^2+1)\sqrt{2Q(u(x_2))} > 0 \qquad \forall x \in (x_2, x_3]. \tag{10.26}$$

If $x_3 = \infty$, then (10.26) implies that $u''(\infty) > 0$, contradicting the condition $u''(\infty) = 0$ given in (10.1). Thus, $x_3 < \infty$ and it follows from (10.25) that

$$u'''(x_3) = 0. \tag{10.27}$$

Finally, suppose that

$$u(x_2) < u(x) \leq \bar{u} \qquad \forall x \in (x_2, x_3).$$

Then (10.8) and (10.9) imply that

$$0 \leq Q(u(x)) \leq Q(u(x_2)) \qquad \forall x \in (x_2, x_3). \tag{10.28}$$

Combining (10.26), (10.27), and (10.28), and setting $x = x_3$ in (10.5), we obtain

$$-(b^2-1)(u'(x_3))^2 = \frac{(u''(x_3))^2}{2} - (b^2+1)^2 Q(u(x_3)) > 0,$$

a contradiction since $u'(x_3) > 0$ and $b > 1$. Thus, it must be the case that $u(x_3) > \bar{u} > u(0)$ as claimed. However, as described earlier, this contradicts the fact that $u(x)$ has its global maximum at $x = 0$. This completes the proof.

11. Summary. In this paper we have studied steady states of a partial integro-differential equation that has been used to model working memory in a neuronal network. We have extended previous results for "Mexican hat" coupling to the case where the connectivity function changes sign infinitely often, in the hope of more realistically modeling the connectivity known to exist in the prefrontal cortex. Our main results include (a) a proof of the nonexistence of a type of "multiple bump" solution when the connectivity is of Mexican hat type, (b) an upper bound on the decay rate of an oscillatory connectivity function, above which only trivial solutions exist, and (c) a numerical investigation of the possible solutions and the bifurcations they undergo for a particular oscillatory connectivity function.

For the one-dimensional model, many of the numerical results were obtained as a result of noting that stationary solutions of the partial integro-differential equation (5.1) are equivalent to homoclinic orbits in the related fourth order ordinary differential equation problem (5.8). This property allowed us to use the software package AUTO97 [12, 13], with its facilities for continuing homoclinic orbits, to follow both stable and unstable solutions as parameters were varied. We are presently pursuing a rigorous proof of existence of the families of N-bump solutions found here. Already,

it has been proved in [23] that any bounded solution of the ordinary differential equation in (5.8) also is a solution of the integral equation (5.1). Thus, in addition to homoclinic orbits, we are also investigating the existence of other families of solutions, including periodic, aperiodic, and chaotic solutions. While many of our results were derived by exploiting the specific form of an oscillatory connectivity function, we believe that the qualitative aspects of our results will hold for any qualitatively similar function.

For the two-dimensional extension of our model we used a MATLAB [28] code to generate stable multi-bump solutions. For appropriate parameter values we found that N-bump solutions exist and that they retain many of the characteristic qualities of solutions of the one-dimensional model. However, we also found stable solutions which were not predicted by our one-dimensional studies. In future research we will continue our investigation of the different types of stable patterns of solutions of the two-dimensional problem.

Acknowledgment. The authors thank Edward Krisner and the referees for making several helpful suggestions.

REFERENCES

[1] S. Amari, *Dynamics of pattern formation in lateral-inhibition type neural fields,* Biol. Cybern., 27 (1977), pp. 77–87.
[2] S. Amari, *Mathematical Theory of Neural Networks,* Sangyo-Tosho, Tokyo, 1978.
[3] D. J. Amit and N. Brunel, *A model of global spontaneous activity and local structured activity during delay periods in the cerebral cortex*, Cereb. Cortex., 7 (1997), pp. 237–252.
[4] P. C. Bressloff, *Travelling fronts and wave propagation failure in an inhomogeneous neural network,* Phys. D, 155 (2001), pp. 83–100.
[5] A. R. Champneys, *Homoclinic orbits in reversible systems and their applications in mechanics, fluids and optics,* Phys. D, 112 (1998), pp. 158–186.
[6] A. R. Champneys, *Homoclinic orbits in reversible systems* II*: Multibumps and saddle centers,* CWI Quarterly, 12 (1999), pp. 185–212.
[7] A. R. Champneys and P. J. McKenna, *On solitary waves of a piecewise linear suspended beam model,* Nonlinearity, 10 (1997), pp. 1763–1782.
[8] C. L. Colby, J. R. Duhamel, and M. E. Goldberg, *Oculocentric spatial representation in parietal cortex,* Cereb. Cortex., 5 (1995), pp. 470–481.
[9] A. Compte, N. Brunel, P. Goldman-Rakic, and X.-J. Wang, *Synaptic mechanisms and network dynamics underlying spatial working memory in a cortical network model,* Cereb. Cortex., 10 (2000), pp. 910–923.
[10] S. Coombes, G. J. Lord, and M. R. Owen, *Waves and Bumps in Neuronal Networks with Axo-Dendritic Synaptic Interactions,* preprint, Loughborough University, Leicestershire, UK, 2002.
[11] M. C. Cross and P. C. Hohenberg, *Pattern formation outside of equilibrium,* Rev. Modern Phys., 65 (1993), pp. 851–1112.
[12] E. J. Doedel. *Auto: A program for the automatic bifurcation analysis of autonomous systems,* in Proceedings of the Tenth Manitoba Conference on Numerical Mathematics and Computing, University of Manitoba, Winnipeg, Canada, 1981, pp. 265–284.
[13] E. Doedel, A. R. Champneys, T. F. Fairgrieve, Y. A. Kuznetsov, B. Sandstede, and X. Wang, *AUTO*97*: Continuation and Bifurcation Software for Ordinary Differential Equations (with HomCont)*, report, CMVL, Concordia University, Montreal, 1997.
[14] G. B. Ermentrout, *Neural networks as spatio-temporal pattern forming systems,* Rep. Progr. Phys., 61 (1998), pp. 353–430.
[15] S. Funahashi, C. J. Bruce, and P. S. Goldman-Rakic, *Mnemonic coding of visual space in the monkey's dorsolateral prefrontal cortex,* J. Neurophysiol., 61 (1989), pp. 331–349.
[16] B. Gutkin, G. B. Ermentrout, and J. O'Sullivan, *Layer* 3 *patchy recurrent connections may determine the spatial organization of sustained activity in the primate frontal cortex,* Neurocomputing, 32–33 (2000), pp. 391–400.
[17] M. A. Giese, *Dynamic Neural Field Theory for Motion Perception,* Kluwer Academic, Boston, 1998.

[18] Y. Guo and C. Chow, *Localized Persistent States in Neural Networks,* preprint, University of Pittsburgh, Pittsburgh, PA, 2002.
[19] D. Hansel and H. Sompolinsky, *Modeling feature selectivity in local cortical circuits,* in Methods in Neuronal Modeling, 2nd ed., C. Koch and I. Segev, eds., MIT Press, Cambridge, MA, 1998.
[20] P. Hirschberg and E. Knobloch, *Šil'nikov–Hopf bifurcation,* Phys. D, 62 (1993), pp. 202–216.
[21] G. W. Hunt, M. A. Peletier, A. R. Champneys, P. D. Woods, M. Ahmer Wadee, C. J. Budd, and G. L. Lord, *Cellular buckling in long structures,* Nonlinear Dynam., 21 (2000), pp. 3–29.
[22] K. Kishimoto and S. Amari, *Existence and stability of local excitations in homogeneous neural fields,* J. Math. Biol., 7 (1979), pp. 303–318.
[23] E. Krisner, W. Troy, and C. R. Laing, *N–Bump Solutions of a Model of Short Term Memory,* manuscript, 2002.
[24] C. R. Laing and C. C. Chow, *Stationary bumps in networks of spiking neurons,* Neural Comp., 13 (2001), pp. 1473–1494.
[25] C. Laing and P. Glendinning, *Bifocal homoclinic bifurcations,* Phys. D, 102 (1997), pp. 1–14.
[26] J. B. Levitt, D. A. Lewis, T. Yoshioka, and J. S. Lund, *Topography of pyramidal neuron intrinsic connections in macaque monkey prefrontal cortex (areas* 9 *and* 46*),* J. Comp. Neurol., 338 (1993), pp. 360–376.
[27] D. A. Lewis and S. A. Anderson, *The functional architecture of the prefrontal cortex and schizophrenia,* Psychol. Med., 25 (1995), pp. 887–894.
[28] Matlab, The MathWorks, Natick, MA.
[29] E. K. Miller, C. A. Erickson, and R. Desimone, *Neural mechanisms of visual working memory in prefrontal cortex of the Macaque,* J. Neurosci., 16 (1996), pp. 5154–5167.
[30] L. A. Peletier and W. C. Troy, *Patterns: Higher order models in physics and chemistry,* Birkhäuser, Boston, 2001.
[31] J. G. Taylor, *Neural "bubble" dynamics in two dimensions: Foundations,* Biol. Cybern., 80 (1999), pp. 393–409.
[32] E. Thelen, G. Schöner, C. Scheier, and L. B. Smith, *The dynamics of embodiment: a field theory of infant perseverative reaching,* Behavioral and Brain Sciences, 24 (2001), pp. 1–34.
[33] W. C. Troy and C. R. Laing, *Two–bump solutions of Amari's model of working memory*, Phys. D, submitted.
[34] M. Usher, M. Stemmler, and Z. Olami, *Dynamic pattern formation leads to 1/f noise in neural populations,* Phys. Rev. Lett., 74 (1995), pp. 326–329.
[35] X. J. Wang, *Synaptic basis of cortical persistent activity: The importance of NMDA receptors to working memory,* J. Neurosci., 19 (1999), pp. 9587–9603.
[36] H. Werner and T. Richter, *Circular stationary solutions in two–dimensional neural fields,* Biol. Cybern., 85 (2001), pp. 211–217.
[37] H. R. Wilson and J. D. Cowan, *A mathematical theory of the functional dynamics of cortical and thalamic nervous tissue,* Kybernetik, 13 (1973), pp. 55–80.
[38] P. D. Woods and A. R. Champneys, *Heteroclinic tangles and homoclinic snaking in the unfolding of a degenerate reversible Hamiltonian–Hopf bifurcation,* Phys. D, 129 (1999), pp. 147–170.
[39] K. Zhang, *Representation of spatial orientation by the intrinsic dynamics of the head–direction cell ensemble: A theory,* J. Neurosci., 16 (1996), pp. 2112–2126.